STABILITY ANALYSIS OF A NON-MINIMUM PHASE ELECTRO-HYDRAULIC SERVO SYSTEM (EHSS) AND IDENTIFICATION OF PARAMETRIC UNCERTAINTY

By

Mazid Ishtique Ahmed

12261002

Master of Science in Electrical and Electronic Engineering

Department of Electrical and Electronic Engineering

Brac University

December 2021

STABILITY ANALYSIS OF A NON-MINIMUM PHASE ELECTRO-HYDRAULIC SERVO SYSTEM (EHSS) AND IDENTIFICATION OF PARAMETRIC UNCERTAINTY

By

Mazid Ishtique Ahmed
12261002

A thesis submitted to the Department of Electrical and Electronic Engineering in partial fulfillment of the requirements for the degree of
Master of Science in Electrical and Electronic Engineering (M.Sc. in EEE)

Department of Electrical and Electronic Engineering
Brac University
December 2021

Declaration

It is hereby declared that

1. The thesis submitted is my own original work while completing degree at Brac University.
2. The thesis does not contain material previously published or written by a third party, except where this is appropriately cited through full and accurate referencing.
3. The thesis does not contain material which has been accepted, or submitted, for any other degree or diploma at a university or other institution.
4. I have acknowledged all main sources of help.

Student's Full Name & Signature:

Mazid Ishtique Ahmed
12261002

Approval

The thesis titled "STABILITY ANALYSIS OF A NON-MINIMUM PHASE ELECTRO-HYDRAULIC SERVO SYSTEM (EHSS) & IDENTIFICATION OF PARAMETRIC UNCERTAINTY" submitted by

1. Mazid Ishtique Ahmed (12261002)

of Spring, 2017 has been accepted as satisfactory in partial fulfillment of the requirement for the degree of Master of Science in Electrical and Electronic Engineering on December 5, 2021.

Examining Committee:

Supervisor:
(Member)

Dr. A.K.M. Abdul Malek Azad
Professor, Electrical and Electronic Engineering
Brac University

Internal Expert Examiner:
(Member)

Dr. Abu Hamed M. Abdur Rahim
Professor, Electrical and Electronic Engineering
Brac University

External Expert Examiner:
(Member)

Dr. Shahnewaz Siddique
Assistant Professor, Electrical and Computer Engineering
North South University

Departmental Head:
(Chair)

Dr. Md. Mosaddequr Rahman
Professor and Chairperson, Electrical and Electronic Engineering
Brac University

Ethics Statement

This is to certify that this thesis titled STABILITY ANALYSIS OF A NON-MINIMUM PHASE ELECTRO-HYDRAULIC SERVO SYSTEM (EHSS) & IDENTIFICATION OF PARAMETRIC UNCERTAINTY" is the result of my study for partial fulfillment of Master of Science in Electrical and Electronic Engineering degree under supervision of Dr. A.K.M. Abdul Malek Azad, Professor, Department of Electrical and Electronic Engineering, Brac University and no part of this work has been submitted elsewhere partially or fully for the award of any other degree or diploma. Parts of this thesis have been published as two conference papers, of which one in IEEE TENCON 2016, Singapore and another is accepted in IEEE TENCON 2021, New Zealand. Any material reproduced in this thesis dissertation has been properly acknowledged.

Abstract

The electro-hydraulic servo system (EHSS) is a common tool in a variety of modern-day industrial applications that mostly deal with aviation and vehicle manufacturing and operation. In this thesis, an electro-hydraulic servo system is presented which bears the characteristics of non-minimum phase (NMP) phenomenon. A discrete-time transfer function for investigating the EHSS-NMP features has been estimated using a revamped mathematical model of the EHSS with respect to existing model parameters. An optimal control strategy is then formulated based on discrete linear quadratic regulator (DLQR) that seemingly, optimizes the control issues associated with EHSS affected by NMP behavior. A comparative analysis shows that the EHSS stability response improves with the DLQR, but the NMP behavior still persists. This thesis also tries to identify parametric uncertainties through a comprehensive mathematical model of EHSS. The modeling constraints are then investigated to propose a finite frequency robust control technique to actuate an active suspension load subjected to road disturbances. Using various performance criteria, simulation results are able to determine an optimum trade-off between robust control and rejecting road disturbances at higher deflection frequencies. As a result, these studies have demonstrated that the proposed control technique may overcome the parametric uncertainties of an EHSS-driven active suspension load.

Keywords: EHSS, NMP, DLQR, Uncertainties, Robust, Active Suspension

Dedication

With the grace of Almighty, I have completed the thesis work being inspired by many. But I dedicate my work to my loving daughter Mehvish Inshirah Ahmed.

.

Acknowledgement

I would like to sincerely express my deepest thanks and gratitude to my supervisor, Dr. A.K.M. Abdul Malek Azad, Professor, Department of Electrical and Electronic Engineering (EEE) of Brac University for his continuous support and guidance for completing my M.Sc. in EEE thesis work.

I would also like to thank the Dean of School of Engineering, Brac University, the Chairperson, Department of EEE, Brac University and the Program Coordinator, Post Graduate Program, Department of EEE, Brac University for their co-operation.

Table of Contents

List of Figures

List of Tables

List of Acronyms

NMP	Non-Minimum Phase
EHSS	Electro-Hydraulic Servo System
EHSV	Electro-Hydraulic Servo-valve
DLQR	Discrete Linear Quadratic Regulator
PDE	Partial Differential Equation
RODE	Riccati Ordinary Differential Equation
HJB	Hamiltonian-Jacobi-Bellman Equation

Chapter 1

Introduction

1.1 Background and Motivation

The combination of electronic control and hydraulic power systems has resulted in significant amount of formidable and rigorous control systems, benefiting the overall fluid engineering technically and economically. Electro-hydraulic servo system (EHSS) is considered as one of the leading solutions for process control in heavy engineering industries for the past few decades. It is comprised of a pump, an accumulator, a relief valve, a servo-valve and a hydraulic actuator as the primary parts. The servo-valve is one of the staple components of the entire system which generates the power to control flow direction, force, pressure, position, speed and acceleration. Position tracking is one of the common applications for EHSS which has been widely adapted in operation of aircraft, automotive, robotics etc.

Process automation research in a variety of sectors has shown that electro-hydraulic control systems offer the smallest possible actuator size and mass while providing the highest possible output power and speed, all while providing the ease of computer control. Thus, electro-hydraulic control systems are becoming more prevalent in sectors such as automated production systems (FAPS), robotic aggregate, automatic machines, construction and road equipment, shipbuilding, aviation, and other technological industries. Significant advancements in missile penetration avoidance technology, as well as the promotion of the fast development of warhead penetration technology, have occurred in recent years among key military forces across the globe and in control and monitoring, these systems replace solely mechanical and electrical systems because they combine the well-known benefits of electrical communications and control with the speed and relative ease of strong hydro-pneumatic motors [1].

Technological advances in servo control, which include electro-hydraulic servo control, are becoming more significant in the field of automation, and it is now regarded to be one of the most important basic technologies in mechatronics. The vast majority of these systems are composed of hydraulic drives that use valve-controlled actuation, although the rate of energy consumption is still considerably lower than average. The pump-control system with volumetric control may significantly increase the durability of such systems; however, the lag in reaction speed causes the control precision to be unsatisfactory [2]. Many studies concentrated on just one of the two goals of high control accuracy or high energy efficiency in the electrohydraulic system: high control accuracy or high energy efficiency. The valve control technique, which employs an advanced nonlinear control scheme, is often used to attain high levels of control precision [3].

Powerful electro-hydraulic servo control systems are almost inexorably connected to control systems that need quick response times and high accuracy. Since the publication of Merritt's "Hydraulic Control Systems" in 1967, the conventional electro-hydraulic servo control has undergone a systematic development process.

The approaches based on traditional electro-hydraulic servo control continue to be the most frequently utilized control systems in the industrial and military sectors as of right now, according to industry statistics. Interference from inside and outside a system are two instances of uncertainty that may have a major effect on the operation of a system. Position tracking is one of the most common industrial applications requiring EHSS, however, despite being advantageous for complex applications, such systems require extensive consideration regarding that control technique to be adopted, due to suffering from inherent characteristics of non-minimum phase (NMP) systems. As a result, EHSS is also susceptible to a wide range of disturbances, including parametric errors and unknown disturbances, which makes trajectory tracking for position control under high inertial load very challenging [4].

The performance of an electro-hydraulic servo system is often hampered by parameter uncertainties and mismatched random disturbances, which are two of the most significant barriers to attaining high-performance servo control performance [5].

This phenomenon causes the initial response of such systems to be delayed due to dead time. Thus, in spite of the forward system being causal and stable, the corresponding inverse becomes unstable resulting NMP behavior. It is commonly observed in control approaches towards EHSS inheriting all the design complexities. According to the discussions above, a range of control techniques are employed in the optimization of the control performance of a force control system, and the control effect is very excellent. In addition, although the control effectiveness is very good, the complexity of the control models, the efficacy of the force control technique in engineering practice has to be confirmed in more extensive testing.

1.2 Literature Review

Position tracking performance of EHSS highly relies on the accuracy of tracking and robustness of the overall control approach which can only be assured by the compensation of NMP characteristics. Challenges in designing the perfect controlling mechanism for position tracking control of EHSS have largely attracted researchers' attention from around the globe and are implemented and documented in various journals and scientific artic1es.

The control strategies of EHSS have been a highlighted topic of interest for many researchers due to its operational characteristics exhibiting non-minimum phase behavior. The nonlinearities of the EHSS invoked by the NMP characteristics are being addressed by researchers for a long. Although feedback linearization techniques were employed with closed-loop optimal feedback control strategy in many articles, these were proved not to be robust in modeling uncertainty and sensor noise due to the high-order derivative terms in control inputs [6]. With established advantages of sliding mode control strategy for obtaining robust control of such system behavior to stabilize the overall parameter tracking under influence of external disturbances, it was also found that in practice, the upper bound is partly known or even completely unknown, so the switching gains must be sufficiently large to suppress the influence of the uncertainties [7].

In [8], the difficulties in designing the optimal controlling mechanism for position tracking control of EHSS have also largely attracted the attention of researchers from all over the world, who have implemented and documented their findings in a number of scientific journals and articles published in professional journals. Over the last several decades, a significant amount of work linked to EHSS has suggested linear, intelligent, and non-linear control methods, such as Perfect-Tracking optimum control, that have been implemented.

In [9], it was proposed to create a nonlinear adaptive robust control for the valve-controlled hydraulic system that is based on adaptive robust control and discrete disturbance estimating techniques. Unknown linear or nonlinear parameters are among the uncertainties taken into consideration in this study. Meanwhile, a nonlinear adaptive robust control law is derived using a particular Lyapunov function, which not only ensures that state variables and control signals are bounded but also adjusts for the effects of parameter uncertainties, external disturbances, and mistakes in parametric estimations. The suggested control system is then tested using computer simulations under different operating circumstances to ensure that it has good dynamic performance and is resistant to failure.

In [10], the modeling and simulation of a nonlinear inverted pendulum-cart dynamic system utilizing a proportional-integral-derivative (PID) controller and a linear quadratic regulator (LQR) with the purpose of determining the optimum control scheme. To control the nonlinear dynamical system, this article employed two techniques: LQR, a best-effort control approach, and the proportional-integral-derivative (PID) control method, both of which were often used for the management of linear dynamical systems. It was necessary to feed the nonlinear system states to the LQR, which was built using the linear state-space model. When developing control techniques, the inverted pendulum, a highly nonlinear unstable system, is utilized as a benchmark to ensure that they are effective which resonated the usefulness of LQR in controlling non-linear systems.

In [11], the impact of external disturbance on the servo-valve position tracking of electro-hydraulic servo system within a certain frequency range by taking all parameter uncertainties under consideration for establishing the mathematical model was presented. The authors modeled a Finite Frequency H∞ disturbance observer actuating a classical PID controller to overcome the uncertainties by suppressing the interference effects within model-specific frequency domain.

A similar model uncertainty for systems with NMP characteristics was explored in [12], where the authors proposed a robust disturbance rejection methodology for such unstable NMP systems. Initially, the internal stability was analyzed and based on findings of stability criterions resulting several constraints, it was proposed to obtain robust stability by designing, trade-offs among these constraints which eventually brought the system to operate with less conservatism and better performance in specified frequency range. The parameter optimization was obtained with a disturbance rejection filter for extended frequency range of a H∞ disturbance observer by loop shaping method to push the zeroes of the NMP systems within the unit circle in z-plane.

The active disturbance rejection control mechanism was also explored in [13], to improve the position tracking performance of the electro-hydraulic actuation system in the presence of parametric uncertainties, non-parametric uncertainties, and external disturbances as well. The authors proposed the disturbance observers (Dos) to estimate not only the matched lumped uncertainties but also mismatched disturbances based on the high-order Levant's exact differentiator. These disturbances were integrated into the control design system based on the backstepping framework which showed higher accuracy in servo-valve position tracking performance. The system stability was analyzed by using Lyapunov stability theory and the results concluded in the presence of time-varying parametric uncertainties and external load disturbances.

1.3 Electro-Hydraulic Servo System – at a glance

Due to their rapid response, high control precision, and massive power transmission capabilities, electro-hydraulic servo systems are widely employed in modern industrial applications such as a parallel robot platform [14], automotive suspension system [15], hydraulic load emulator, and so on. However, model uncertainties in the hydraulic system are always present due to complex flow–pressure features of the control valve, oil compressibility, and leakage [16]. In addition, there are some hard nonlinearities in the hydraulic system, such as control input saturation, dead zone nonlinear friction, and so on [17]. As a result, the response of EHSS shows non-minimum phase properties due to the excessive delay between the stimulus and the corresponding response, which is called transmission delay or dead time.

The phase response of the system is the result of the analysis in the frequency domain, and based on the poles and zeros obtained from the transfer function of the analysis in the frequency domain, if one or more zeroes are found in the right half of s-plane for continuous time transfer function or any zero outside of the unit circle on the z-plane for discrete time transfer function, the system is called non-minimum phase system.

Servo-valves are employed in closed-loop control systems which are the fundamental part of EHSS. When used as standalone, it refers to a system in which a low-power input signal is amplified to produce a controlled high-power output or signal that is used to drive a mechanical load of large mass that is subjected to environmental disturbances. Almost all hydraulic and mechanical parameters, such as pressure, pressure difference, angular speed, displacement, angular displacement, strain and force are controlled by them.

The model of reference for EHSS for understanding its mechanical structure and principle of working is presented as an aircraft fin actuator. It controls the lateral/vertical movement of any aircraft. The airplane movement fin is depicted as the load in Fig. 1.1 of the EHSS schematic layout.

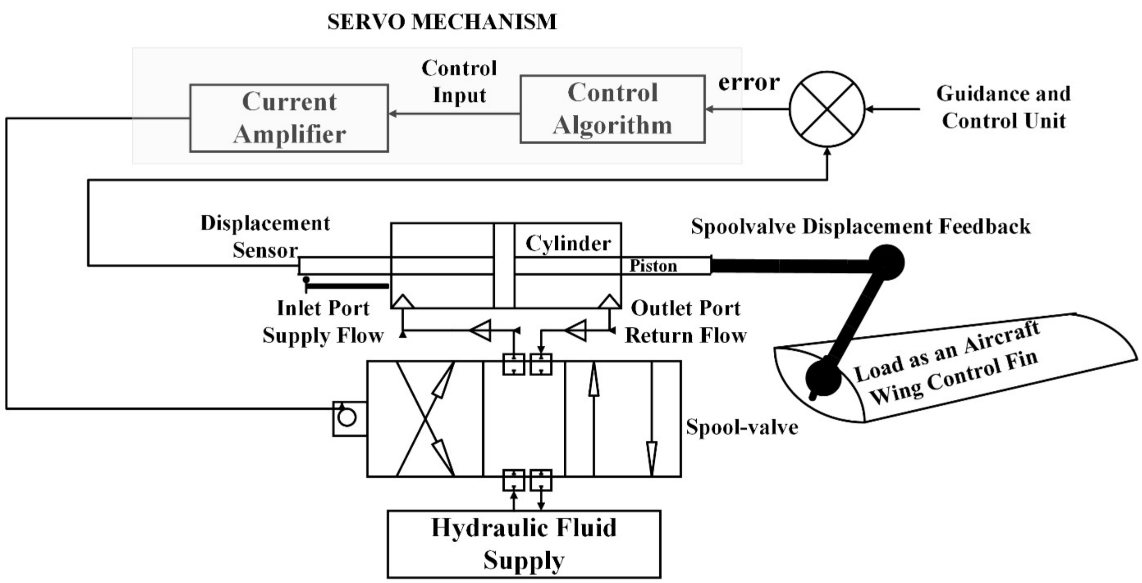

Fig. 1.1 Schematic Diagram of Fin position Servo System based on EHSS

The input current is adjusted to actuate the cylinder into the desired position. The servo-controller then compares the position input to the voltage input, generating input current proportional to the difference between the input voltage and the voltage output of the position sensor. The torque motor of the servo-valve, which is operated by the provided input current, subsequently controls the spool displacement.

The rate of flows as well as the direction of the flows provided to each cylinder chamber are determined by the position of the spool-valve and the circumstances of the piston's load (in this example, the aircraft fin). These variations in flow pressure, in turn, determine the piston's ultimate motion. Servo-valve allows the flow of hydraulic fluid from the hydraulic power supply unit to the load using the fluid for further mechanical movement. Thus, the position control of the servo-valve is actuated.

Fly-by-Wire is a method of controlling the control surface of an airplane using actuators that operate at high hydraulic pressure. Similar to that, Brake-by-Wire technology is also seen as a viable solution for high-speed racing cars. For both of these hydraulic driven systems are commonly controlled by the means of EHSS. The operation as explained above is illustrated as block diagram in Fig. 1.2.

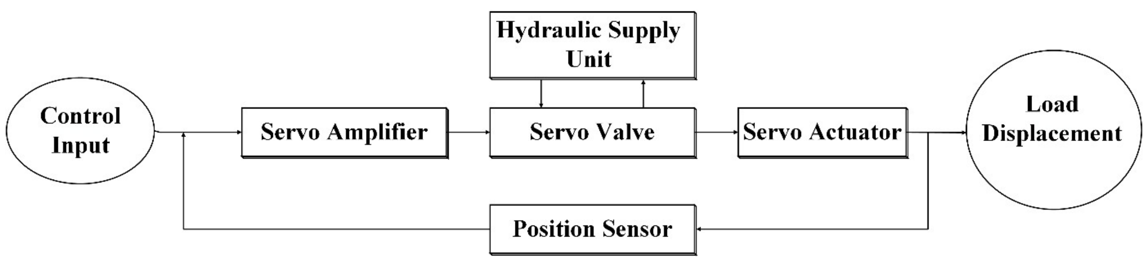

Fig. 1.2 Block Diagram of EHSS operation

1.4 Stability Properties of Non-Minimum Phase Systems

Frequency domain analysis of system properties through transfer function can indicate several particulars including stability of response by the positions of poles and zeros on the complex s-plane as well as for discrete time analysis on z-plane [18]. System characterizations can be done based on parametric response and are classified as minimum phase systems, all pass systems and non-minimum phase systems and types of each of them can be found through pole-zero plot of respective transfer functions.

The transfer functions of minimum phase systems have all poles and zeros in the left side of the s-plane. The transfer functions of all pass systems have a pole-zero pattern that is anti-symmetric about the imaginary axis. Non-minimum phase systems are those whose continuous time transfer functions have one or more zeros in the right half of the s-plane. On the other hand, for corresponding discrete time transfer function, if one or more zeroes lie outside of the unit circle on the z-plane, the system is also characterized as non-minimum phase [19].

Because the transfer function (TF) of a non-minimum Phase (NMP) system cannot be derived just from the magnitude curve, it has various operational difficulties. The internal stability of the system is affected by a drastic phase response compared to a steady magnitude curve over the full frequency range, resulting in more than one zeroes outside of the z-plane [20].

1.5 Problem Statement

The electro-mechanical operation of EHSS as described above in section 1.2 through various literature of previous research works has the non-linear system properties. In spite of, being very popular in mission critical industrial applications such as aerospace, automobile, process manufacturing etc., EHSS is very difficult to be operated with precision. In addition to that, modern day systems are highly actuated through digital systems for better operation and maintenance services and EHSS being controlled by discrete-time signal requires to be similarly capable. In order to devise a tracking control strategy taking all these performance indicators into account for the optimum exertion of response on the load subjected to disturbances posed by the surroundings, it is necessary to transform the physical nature of this electro-mechanical system part by part mathematical model. The mathematical model through simulation works will then provide the useful insight of these issues of NMP and the stability criterions of the operation of the EHSS which as a result will specify the parameters responsible for causing these control issues. Based on the nature of these issues, appropriate control strategy employing discrete-time control signal will be investigated through simulation environment of MATLAB/SIMULINK along with the observations of the limitations of the adopted solution. Therefore, a complete control strategy to overcome the NMP properties of EHSS is necessary to be explored, rigorously.

1.6 Objectives

The primary objective of this work is to identify the parameters that contribute to cause the non-minimum phase response of electro-hydraulic servo system (EHSS) to understand the stability. To achieve that goal, understanding of the physical phenomenon of EHSS requires to be studied which is obtained by mathematical modeling, excluding the unknown system parameters as well as any external disturbances caused by the driving load. Properties of EHSS in frequency domain are then analyzed by the system's characteristics exhibiting non-minimum phase behavior through pole-zero position over the z-plane. Optimal control strategy is then adopted to improve the stability of the response observed in the open-loop response of the EHSS by computing a feedback gain. The closed-loop condition is then to be evaluated to understand the improvement in NMP phenomenon. Finally, the overall stability of the EHSS is to be re-evaluated by comprehensive mathematical modeling inclusive of un-modeled parameters and external disturbances caused by the load to identify the parametric uncertainties.

1.7 Organization of the Dissertation

The rest of this dissertation is organized as detailed below –

Chapter 2: Mathematical Modeling of Electro-Hydraulic Servo System (EHSS) with Known Model Parameters

In this chapter, the operational principle of EHSS will be presented in consideration of known system parameters only to constitute the open-loop transfer function. The pole-zero positions on the z-plane will also be analyzed to understand the non-minimum phase (NMP) feature contributing to EHSS's performance in terms of stability through simulated results.

Chapter 3: Optimal Control using Discrete Linear Quadratic Regulator (DLQR)

In order to find out improvement in response stability of EHSS suffering from NMP properties, this chapter will discuss the modeling of a discrete linear quadratic regulator (DLQR) as a feedback controller for optimizing the spool-valve displacement. At the end of this chapter, the closed-loop performance of EHSS supported by the DLQR will be shown to understand the performance gain as well as the limitations.

Chapter 4: Identification of Parametric Uncertainties for EHSS

This chapter will present the identification of unknown model parameters coupled with the effect of external disturbances on the overall stability of EHSS. The comprehensive mathematical modeling of EHSS will then be used to determine the parametric uncertainties through simulation models.

Chapter 5: Conclusion and Future Research Scope

In this last chapter the main results of this dissertation will be summarized with concluding remarks by proposing potential directions for future research of control strategy solution.

Chapter 2

Mathematical Modeling of Electro-Hydraulic Servo System (EHSS) with Known Model Parameters

2.1 Introduction

In this chapter the mathematical modeling of the electro-hydraulic servo system (EHSS) is presented in details using the known system parameters. The mathematical modeling discusses by initially explaining the operational principle of the EHSS through the mathematical deduction of its mechanisms. The mathematical model is thus obtained by numerically developing its transfer function. The step response is then analyzed while the issues of the NMP phenomenon are addressed by observing the pole-zero plot.

2.2 Operational Principle of EHSS

Electro-hydraulic servo system (EHSS) as has been outlined in 1.3, consists of a single-rod cylinder, a 4/3-way servo-valve, and a mass load. The corresponding parameters of the physical model illustrated in Fig. 1.1 are represented in the schematic representation in Fig. 2.1 [21]. A hydraulic power supply unit (e.g., motor, pump, accumulator, pressure meter, and reservoir), Servo-valve, double-ended hydraulic cylinder, load, position sensor, and amplifier make up the system. The position tracking control will take place utilizing the actuation of the EHSS, and the control fin is connected with it as the load of the EHSS illustrated in Fig 2.1.

The input current is regulated to actuate the cylinder into the desired position. The servo-controller then takes the position input and compares it to the voltage input, generating input current proportional to the error between the input voltage and the position sensor's voltage output. The torque motor of the servo-valve, which is powered by the supplied input current, subsequently controls the spool displacement.

The rate of flows as well as the direction of the flows delivered to each cylinder chamber are determined by the position of the spool-valve and the circumstances of the piston's load (in this example, the aircraft fin). These fluxes, in turn, influence the piston's ultimate motion.

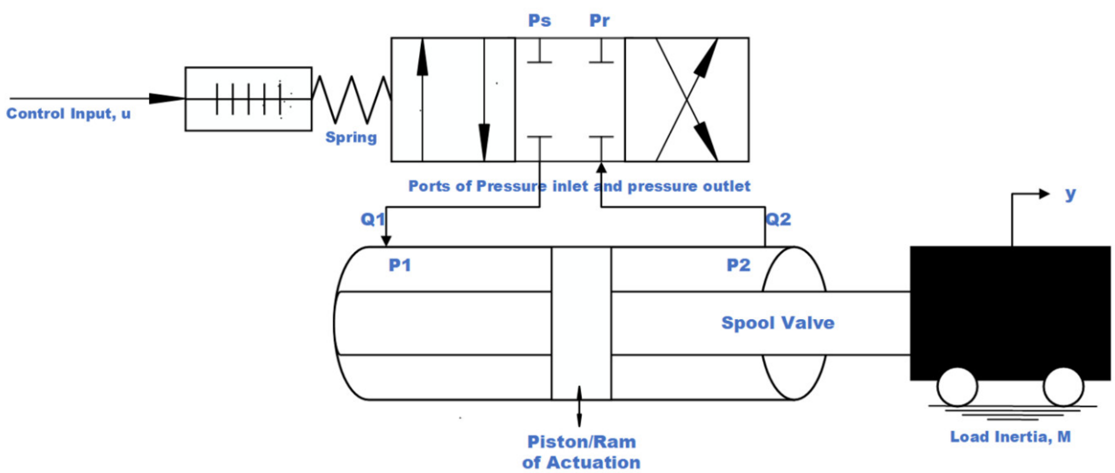

Fig. 2.1 Schematic of EHSS with Load as a Mass-Damper System

2.3 Mathematical Modeling of Open-loop EHSS

Before getting the overall model of the EHSS correlating the load, the mathematical models of each component must be established. The torque motor drives the servo-valve throughout the system. A permanent magnet and an electromagnet (armature) circuit make up a spool, which is an electro-mechanical transducer. The torque motor servo-valve's electrical behavior is specified as –

$$V = \frac{dI}{dt} L_C + R_C I \dots \dots \dots (2.1)$$

Where, L_C and R_C are the coil inductance and resistance, respectively. V indicates the control voltage input and the normalized input current for the energizing the coil is denoted by I.

Test functions are used to determine the dynamic behavior of servo-valve, and the dynamics of spool-valve displacement for the EHSS is theoretically represented by an analogous second order differential equation, which is shown in equation 2.2 below.

$$\frac{d^2x}{dt^2} + 2\zeta\omega_n \frac{dx}{dt} + \omega_n{}^2 = I^*\omega_n \dots\dots\dots (2.2)$$

Where, x indicates the spool-valve displacement of the EHSS. ω_n and ζ are the natural frequency and damping ratio of the spool-valve while $I^* = {}^{I}/_{I_{sat}}$ where, I_{sat} is the saturation current of the torque motor. The flow rate of hydraulic fluid through the servo-valve is proportional to the spool motion under constant load circumstances, according to the hydraulic system's characteristics. Under shifting load circumstances, the flow rate via the servo-valve is proportional to the square root of pressure drop.

The geometry of an ideal servo-valve is flawless, resulting in zero leakage flows, and it is represented as –

$$Q = Kx\sqrt{\Delta P_v} \dots\dots.\dots (2.3)$$

Where,

a. K = Flow rate co-efficient,

b. x = servo-valve spool displacement

c. $\Delta P_V = P_S - P_T - P_L$ and P_S, P_T, P_L are the system pressure exerted by the hydraulic fuel supplier tank, the return line pressure (to the tank) and the counter pressure against the system load, respectively. Most commonly available spool-valve configuration is illustrated in Fig. 2.2 [22].

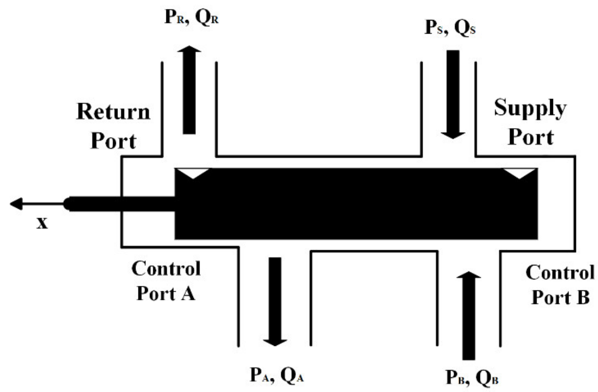

Fig. 2.2 Spool-valve Displacement due to Pressure Dynamics

As a result of equation (2.3), the dynamics of the EHSS operation is obtained by the linearization process using the first-order Taylor series expansion and of the computation of the related Jacobian matrices [23].

$$Q_L = W_q u - W_c P_L \dots \dots \dots (2.4)$$

The total load flow through the actuator divided by the fluid capacitance gives the pressure across the servo actuator piston, and its derivative is given as –

$$P_L = \frac{4\beta_e}{V_t}\left(Q_L - C_{tp}P_L - A_P\dot{y}\right) \dots \dots \dots (2.5)$$

Servo actuator force is thus calculated as –

$$F_a = A_P P_L = M_t \ddot{y} \dots \dots \dots (2.6)$$

Now, by using both equations 2.5 and 2.6, the flow rate variance causing the spool-valve to displace, causing the load to have a similar effect, results in the relationship between excitation and response for the EHSS as a whole and it is shown in equation 2.7 as below.

$$Q_L = \frac{V_t}{4\beta_e}\dot{P}_L + C_{tp}.P_L + A_P.\dot{y} \dots \dots . \dots (2.7)$$

The transfer function of the EHSS represented by these model parameters can now be obtained from equation 2.3 and 2.7 as following in equation 2.8 –

$$\frac{Y(s)}{U(s)} = \frac{K.\omega_n{}^2}{s[s^2 + 2\zeta\omega_n s + \omega_n{}^2]} \dots\dots\dots (2.8)$$

where,

a. $\frac{W_q}{A_P} = K$

b. $A_P{}^2 \frac{4\beta_e}{V_t.M_t} = \omega_n$ and,

c. $\zeta = \frac{\frac{4\beta_e}{V_t.M_t}(W_c+C_{tp})}{2A_P}$

The parameters of equation 2.8 as derived from equation 2.5 to 2.7 are detailed with respective numerical values in Table 1 [24]. The EHSS is comprised mostly of a servo actuator, which serves as its primary control. The size and weight of the actuator are determined by the application for which it is being designed. This particular kind of actuator was selected since the amount of space required is minimal. A frictionless linear bearing is therefore provided to the system workbench, which is fitted with an indirect servo-actuator controlling a spool-valve and a load connected to the end of the rod cylinder. It is as a consequence of this configuration that the nonlinear friction effect during tracking control is reduced. It has a pressure regulator that controls the supply pressure, and the hydraulic oil has been filtered to prevent contamination of the EHSS [25].

Table 1 List of Numerical values of EHS model parameters

Known Model Parameters of EHSS	**Denoted By**	**Numerical Value with Units**
Hydraulic pressure	P_L	$7x10^6$ Pa
Piston surface area	A	$3x10^{-4}$ m^2
Leakage coefficient of the piston	C_{tp}	$2x10^{-12}$
Effective bulk modulus	β_e	$700x10^{-6}$ Pa
Total volume of the compression	V_t	$6x10^{-5}$ m^3
Mass of load	M_t	250 Kg
Flow gain coefficient	K_q	75
Servo-valve gain coefficient	K_c	$1.8x10^{-6}$

2.4 Discrete-time Transfer Function of EHSS with Known Model Parameters

By transforming the continuous time model in equation (2.8) with zero order hold, the equivalent discrete-time model of the system may be derived. The system's discrete time expression is as follows:

$$G(z) = \frac{y(k)}{u(k)} = \frac{b_1 z^2 + b_2 z + b_3}{z^3 + a_1 z^2 + a_2 z + a_3} \ldots\ldots\ldots (2.9)$$

In many investigations, modeling the system in state space model has been accepted as a common approach for computer simulation of the system to get the mathematical model parameters [26]. The discrete time transfer function given in equation (2.9) may be expressed in state space control canonical form as follows using MATLAB simulation based on system identification technique:

$$x(k+1) = Ax(k) + Bu(k) \ldots\ldots\ldots (2.10)$$

$$y(k) = Cx(k) \ldots\ldots\ldots (2.11)$$

Where A, B, C are all positive semi-definite matrices that describe the states, controlled input, and response in the following ways:

$$A = \begin{bmatrix} -a_1 & -a_2 & -a_3 \\ 1 & 0 & 0 \\ 0 & 1 & 0 \end{bmatrix} \ldots\ldots\ldots (2.12)$$

$$B = [1 \quad 0 \quad 0]^T \ldots\ldots\ldots (2.13)$$

$$C = [b_1 \quad b_2 \quad b_3] \ldots\ldots\ldots (2.14)$$

Prior research has relied on discrete-time modeling techniques that were drawn from fundamental principles or physical laws to conduct their investigations. The importance of physical modeling is always addressed in the controller design process; however, validation of the physical plant model in real-world applications is required in order to optimize the use of controllers, which are frequently designed using computer simulation to achieve the best possible results. Furthermore, any changes made to the EHSS's settings may have a detrimental effect on the controller's performance, with the consequence that the intended specification may not be fulfilled as a result of the adjustments. Therefore, system identification utilizing an online estimate technique is always carried out as an adaptive mechanism that interacts with the other control design components in the system identification process. The state-space control canonical form which is computed as shown in equation 2.15 is used to represent the discrete-time transfer function in canonic form, which is derived from the discrete-time transfer function.

$$\left.\begin{array}{c} A = \begin{bmatrix} 3.000 & -3.000 & -0.9999 \\ 1 & 0 & 0 \\ 0 & 1 & 0 \end{bmatrix} \\ B = [1 \quad 0 \quad 0]^T \\ C = [0.7000 \quad 2.800 \quad 0.7000] \end{array}\right\} \ldots\ldots\ldots (2.15)$$

The numerical values of the related known model parameters of the EHSS for the computer simulation are used to determine this discrete time model of the EHSS, and the discrete time transfer function is solved incorporating the equations 2.8 with respective numeric values given in Table 1 is derived as equation 2.16 as given below –

$$G(z) = \frac{0.7z^2 + 2.8z + 0.7}{z^3 - 3z^2 + 3z - 0.9999} \ldots\ldots\ldots (2.16)$$

2.5 Performance Indications of Open-loop EHSS

The transfer function representing the discrete-time dynamics of EHSS with known model parameters in equation 2.16 is used for classifying the EHSS's Servo-valve operation to drive the load as depicted in Fig. 2.1. In order to understand the NMP phenomenon, the pole-zero plot (PZ plot) of this transfer function is observed and shown in Fig. 2.3.

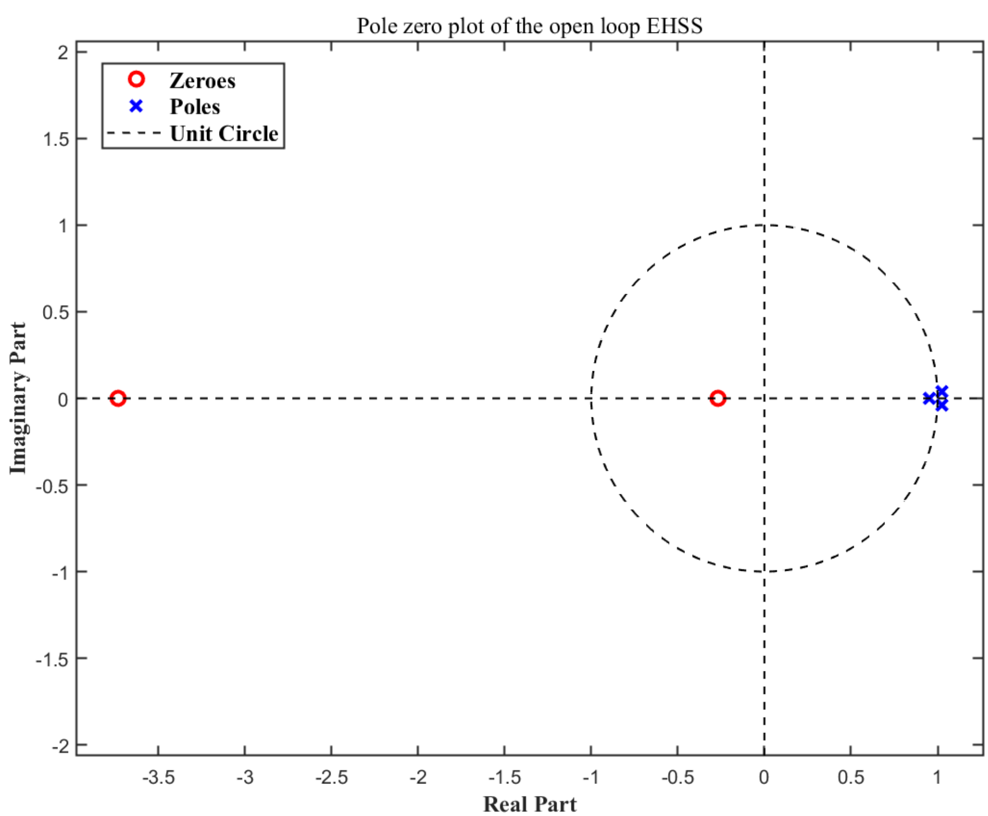

Fig. 2.3 Pole zero plot of EHSS Transfer Function with Known Model Parameters

The PZ plot exhibits two zeroes and three poles on the z-plane. Two of the poles are marginally outside of the unit circle, making the EHSS open-loop response to be critically stable. One zero is obtained outside of the unit circle on the z-plane which is understood to reflect the NMP characteristics of EHSS resulting the response of the system to be delayed as also illustrated in Fig. 2.4.

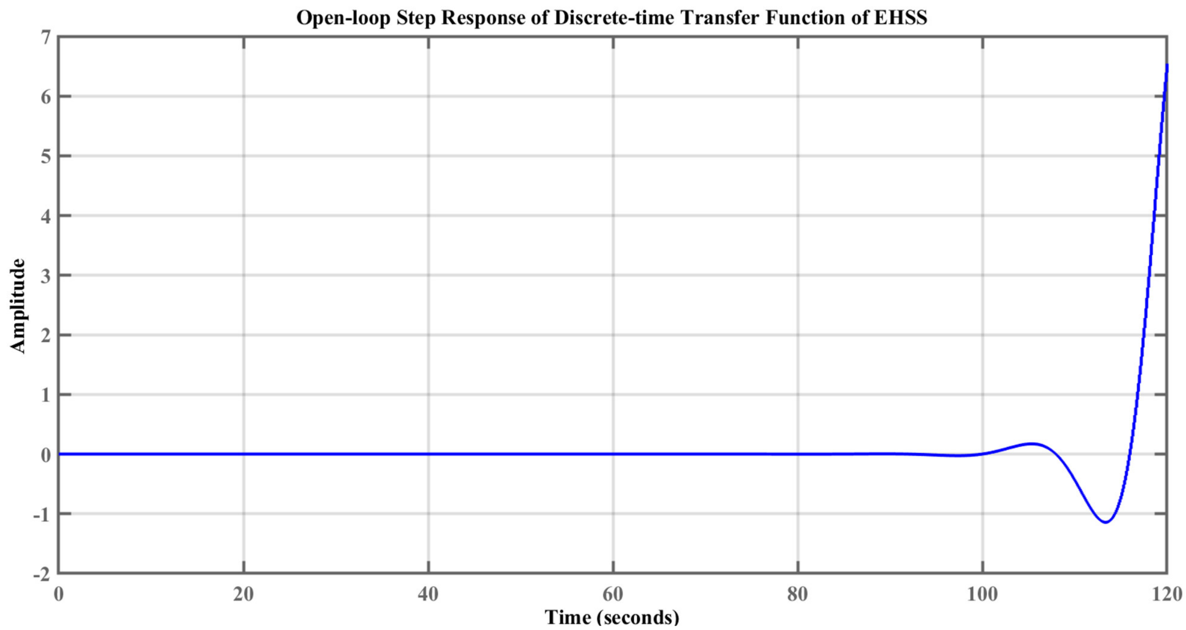

Fig. 2.4 Open-loop Step Response of Discrete-time Transfer Function of EHSS

To understand both of these system behaviors, Fig. 2.5 presents the bode diagram for complete frequency domain representation of the discrete time transfer function as described in equation 2.16. However, the bode diagram also proves that the servo-valve operation exhibits NMP behavior by the graphical illustration of an opposite relation of amplitude response against the phase response. Gradually for the frequency range of 1 to 10 radians per second, the phase lag keeps increasing while the amplitude response is decreasing.

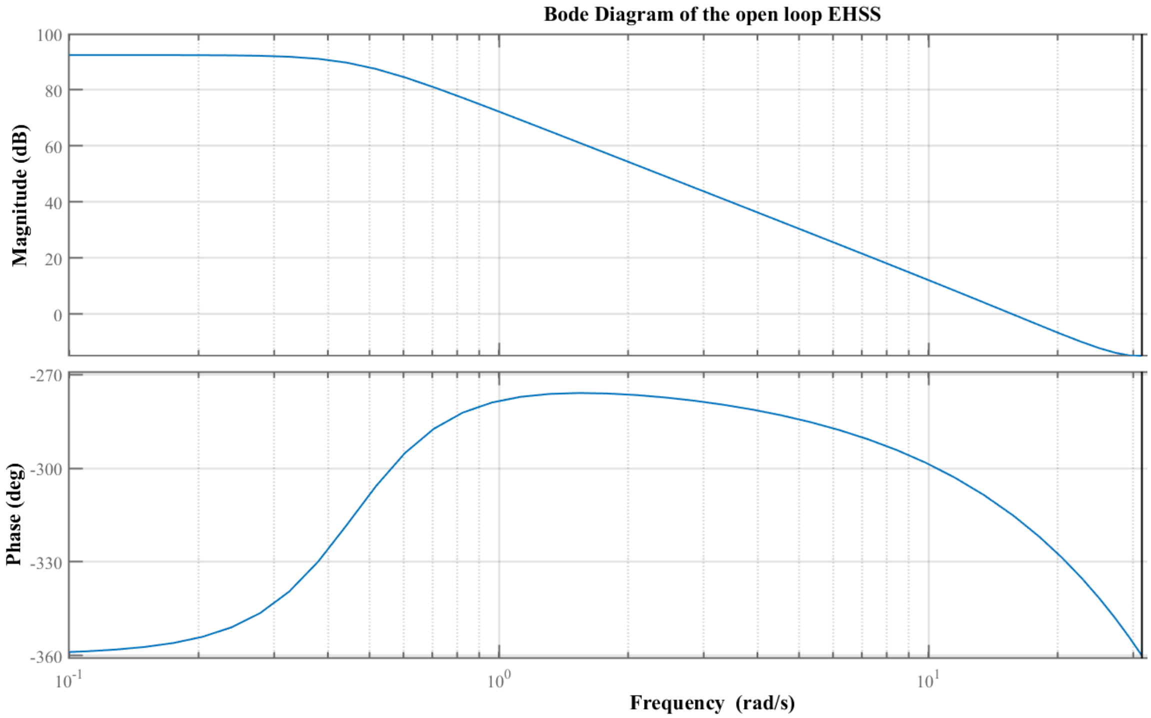

Fig. 2.5 Bode diagram of Open-loop Discrete-time Transfer Function of EHSS

Thus, the system characteristics displaying NMP response can be summarized as it being complex in operational nature which requires to be optimized for improvement in performing mission critical industrial operation. Any unattended delay caused by these issues can lead to mechanical failure due to lack of optimal control in aircraft maneuvering which in result can result into failure of flight control system associated with hydraulic fuel.

In order to address these issues hindering the open-loop response of EHSS, an optimal control strategy is devised through a compensating feedback controller. The mathematical modeling of this optimal control strategy for the mathematically modeled and analyzed EHSS is discussed in the next chapter.

Chapter 3

Optimal Control using Discrete Linear Quadratic Regulator (DLQR)

3.1 Introduction

In this chapter, the mathematical modeling of a discrete linear quadratic regulator (DLQR) is explained to reduce the NMP behavior of the EHSS by Optimizing the performance by developing a closed-loop with on top of the already deduced Discrete-time transfer function (equation 2.15) of the EHSS. The closed-loop step response as well as other performance indicators are compared to understand the advantage of the optimal control technique on EHSS is also presented in this chapter.

3.2 The Discrete Linear Quadratic Regulator (DLQR)

DLQR is a widely used control rule for optimum control, as optimal control is considered the standard approach for solving dynamic optimization issues in systems with non-minimal phase behavior [27]. The resilience of an optimal control strategy based on the DLQR technique against system's uncertain response is one of its fundamental advantages. Due to the high accuracy in achieving trajectory tracking for systems with external disturbances which require rapid change in actuation commonly seen in non-minimum phase systems, DLQR has performance advantage over other optimal control strategies like model predictive control (MPC) [28]. It is widely believed that the most essential feature of both LQR and MPC controllers is closed-loop stability; as a result, both are widely recognized as the best controllers currently available on the market. When compared to the LQR, which optimizes an actual performance index of a closed-loop control system, the MPC explicitly takes into consideration limitations on the parameters in the system, which is an important element in many industrial processes [29].

The objective of this DLQR controller is to acquire the feedback gain for the system to be regulated, as stated in the structure of equations 2.10 and 2.11 such that the cost function mentioned in equation 2.16 is minimized [30].

$$J = \int_{0}^{T} (x^T Q x + u^T R u)dt + x^T(t) H x(t) dt \ldots \ldots \ldots (3.1)$$

Here, the Q ≥ 0, R > 0, H > 0 are symmetric positive semi definite matrices.

3.3 Pontryagin's Maximum Principle for Optimizing the DLQR Cost Function

The cost function stated in equation 3.1 is minimized by deducing the canonical Hamiltonian equation for the given system states for a specified optimal control feedback gain [31]. The Hamiltonian canonical equations are obtained by optimizing the control problem in accordance with the Pontryagin's maximum principle [32]. Essentially, it is regarded as an instantaneous increment of the Lagrangian formulation of the problem to be optimized over a certain time period where the equation 3.2 describes Euler-Lagrangian relation.

$$\frac{\partial L(x, y(x), y'(x))}{\partial y} = \frac{d}{dx}\left(\frac{\partial L(x, y(x), y'(x))}{\partial y'(x)}\right) = 0 \ldots \ldots \ldots (3.2)$$

According to Hamilton's concept of stationary action, the development of an optimal solution for the optimized response of such a system can be derived by the solutions to the Euler equation for the action of the system in Lagrangian mechanics, represented by the functional of $L(x, y(x), y'(x))$ [33]. The Lagrangian function, often known as the Lagrangian quantity, is a quantity that characterizes the state of a physical system, and it is defined as according to mechanics, the Lagrangian function is just the kinetic energy, which is defined as the energy of motion minus the potential energy also defined as the energy of position. The mechanics are a reformulation of classical mechanics that was first presented in the year 1788 by the Italian-French mathematician and astronomer Joseph-Louis Lagrange. Thus, with the knowledge of the Lagrangian for a system, it is possible to determine the action of the system numerically with precision [34].

Optimal control theory makes use of Pontryagin's maximum principle to find the best possible control for moving a dynamical system from one state to another, especially in the presence of constraints for the state or input controls, in order to invoke the stability criterion for systems suffering from the issues described previously for the cases of EHSS which is explained in details as algorithmic steps in the following section of 3.3.1.

3.3.1 Algorithmic Steps of Pontryagin's Maximum Principle

Step 1: Initializing the control inputs and the system states

For a given optimal criterion, considering, $u^* \in U$ is an optimal control excitation. The requirements that must be met in order for a functional to be minimized, it is being assumed that x is the state of the dynamical system with input u. where U denotes the set of controls that are permissible and T denotes the terminal (i.e., final) time of the system.

Step 2: Setting the conditions for the control inputs to corresponding system states

It is necessary to choose the control $u^* = [u_0, u_1, \ldots \ldots, u_i] \in U$ l for all $t \in [0, T]$ in order to minimize the cost functional, which is described in equation 3.1. Also, $x^* = [x_0, x_1, \ldots \ldots, x_i]$ represents the corresponding trajectory for the given control inputs as system states. Here, i is the number of sequences for the control input to indicate the progress parameter of the optimization.

Step 3: Computing the Co-state matrices

Then there is a variable called the costate which together with the known states, satisfies the Hamilton canonical equations as given below in equation 3.3 taking into account the Lagrange multiplier λ.

$$\left.\begin{array}{l} \dot{x} = \nabla_{\lambda} H \\ \lambda = -\nabla_{x} H \end{array}\right\} \ldots \ldots \ldots (3.3)$$

$$\text{where, } H(t, x, u, \lambda) = \lambda^{T}(t) f(x, u, t) + L(t, x, u) \ldots \ldots \ldots (3.4)$$

The relation described in 3.4 depicts that the Hamiltonian functional is computed with respect to the changes in control input, u^{*}if the condition given in the following relation of 3.5 [35].

$$H(t, x^{*}, u^{*}, \lambda^{*}) \leq H(t, x^{*}, u, \lambda^{*}) \ldots \ldots \ldots (3.5)$$

Step 4: Decision on Minimizing the Cost Function

For the duration of time of optimization being constrained as $t_{\text{initial}} = 0$ and $t_{\text{final}} = t_f$ for which the control input assumptions, the cost of $J(u^{*})$ is computed as $J(u_0)$ to $J(u_i)$. The fixed final state for minimizing the cost function, $x(t)$ and $u(t)$, the state variable vector and the control input vector are to be minimized as –

$$\underset{x(t),u(t)}{\text{minimize}} \frac{1}{2} \int_{0}^{t_f} \{x^{T}(t) Q x(t) + u^{T} R u(t)\} dt$$

If, the computed $J(u_i) - Ju_{i-1} > 0$, then the Hamiltonian functional is recomputed as step 3 and a new cost variance is computed as step 4.

Step 5: End of Computation

Else, the progress parameter, i is updated as $i \coloneqq i + 1$ and Step 1 is repeated until the compared minimum of $J(u^{*})$ is achieved.

3.3.2 Computing the Hamiltonian in accordance with Minimized Cost

Subjected to, $x'(t) = Ax(t) + Bu(t)$ as is conventionally presented for the EHSS's state space model for transfer function deduction described in chapter 2.

$$\left.\begin{array}{l} x(t_{initial} = 0) = r_0 \\ x(t_{final} = t_f) = r_f \end{array}\right\} \dots\dots\dots (3.6)$$

For these conditions described in equation 3.4 and 3.6, along with the minimized $J(u^*)$ is thus employed to calculate the Hamiltonian functional being specifically derived as given in equation 3.7.

$$H = -\frac{1}{2}x^T Qx - \frac{1}{2}u^T Ru + \lambda^T(Ax + Bu) \dots\dots\dots (3.7)$$

Now applying the Pontryagin's maximum principle for the maximum condition for the Hamiltonian functional of equation 3.7, the maximum optimized argument for the set of $u^* = u$ is obtained from the relation specified in equation 3.5, as given below in equation 3.8.

$$u^* = \underset{u \in U}{\operatorname{argmax}} \left[-\frac{1}{2}\, u^T Ru + \lambda^{*T} Bu\right] \dots\dots\dots (3.8)$$

Thus, for a single excitation in the system for all $u(t)$ within the constraints of $u_{minimum}$ to $u_{maximum}$ for corresponding $t_{initial} = 0$ and $t_{final} = t_f$, the optimal control input is derived as below in equation 3.9.

$$u^*(t) = \underset{u_{minimum} \le u(t) \le u_{maximum}}{\operatorname{argmax}} \left[-\frac{1}{2}\, r[u(t)]^2 + b\lambda^{*T} u(t)\right] \dots\dots\dots (3.9)$$

Here the statement of equation 3.9 is that the optimal control $u(t)$ maximizes the quadratic factor deduced as $\left[-\frac{1}{2}\, r[u(t)]^2 + b\lambda^{*T} u(t)\right]$. The optimal control $u(t)$ must follow the given constraints as shown in equation 3.10 for $r > 0$ while $r \in R$.

$$u^* = \begin{cases} \frac{b\lambda^*}{r} & ;\ u_{minimum} \leq \frac{b\lambda^*}{r} \leq u_{maximum} \\ u_{minimum} & ;\ \frac{b\lambda^*}{r} < u_{minimum} \\ u_{maximum} & ;\ \frac{b\lambda^*}{r} > u_{maximum} \end{cases} \quad \ldots\ldots\ldots (3.10)$$

Substituting the findings of equation 3.10 in the Hamiltonian canonical equations of the state and costate Functions, thus results into the optimized state and costate equations as shown in equation 3.11, where sat defines the range of saturation for the $\frac{b\lambda^*(t)}{r}$ term.

$$\left.\begin{aligned} \dot{x} &= Ax + b\,\mathrm{sat}_{u_{minimum}}^{u_{maximum}}\left[\frac{b\lambda^*(t)}{r}\right] \\ \dot{\lambda} &= -a\lambda + qx \end{aligned}\right\} \ldots\ldots\ldots (3.11)$$

3.4 DLQR Feedback Gain for the Closed-loop Transfer Function of EHSS

The optimal control strategy for mitigating the disadvantages posed by the NMP behavior of the EHSS in displacement of the spool-valve to operate the load is obtained by deriving a closed-loop transfer function in the presence of a feedback gain, K requires to be solved numerically based on the minimized cost of the function J of equation 3.1 as per the block diagram representation, given in Fig. 3.1 for understanding the improvement in performance through simulated observation.

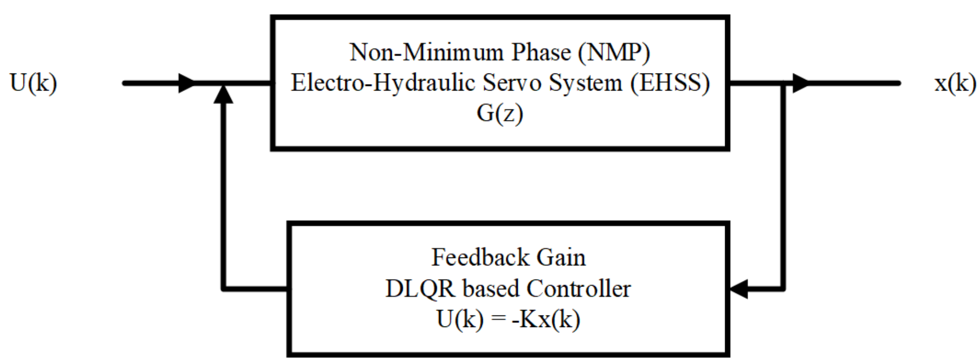

Fig. 3.1 Closed-loop Model of EHSS with DLQR Optimization

To obtain the numerical solution of K, the Hamiltonian functional expressed in equation 3.4 is to be solved incorporating the findings of equation 3.11.

This solution is obtained by applying the Riccati ordinary differential equation solution technique given in equation 3.12 for the discrete-time gain K of DLQR controller which is given in equation 3.13 [36].

$$-\dot{H} = HA + A^T H - HBR^{-1}B^T H + Q \dots\dots\dots (3.12)$$

$$u(t) = -R^{-1}B^T H(t)x \dots\dots\dots (3.13)$$

Where, $K = R^{-1}B^T H(t)$ is the DLQR feedback control gain.

The system matrix A, input matrix B, and output matrix C are utilized in the construction of the DLQR controller, which is based on the discrete-time model of the EHSS defined in equation 2.15 are presented in equation 3.14 below.

$$x(k+1) = A_{cl}x(k) + Bu(k) \dots\dots\dots (3.14)$$

where, $A_{cl} = A - BK$,

The other state matrices of the closed-loop transfer function are also expressed as:

$Q = C^T * C$ and R =1. Here, Q and R both indicate the weight matrices of the input.

Thus, the numeric solution from MATLAB simulation for the DLQR Feedback gain results as illustrated in equation 3.15 which is computed as per the given algorithm steps in Algorithm 1.

$$K = [1.3623 \quad -0.6902 \quad 0.2408] \dots\dots\dots (3.15)$$

Algorithm 1: Computation of DLQR Feedback Gain, K			
1	**Initialize:**	Initial and Terminal Conditions. Finite sequence of iteration $[0, N]$ and Terminal State $x(N)$	
2	**Set:**	Weight Matrices of the System for initial conditions as – $[Q, R, A, B]$	
3		Initial values for Hamiltonian H as H_0^m and Corresponding Gain K as K_0^m	
4	**Compute:**	for: $m \leftarrow N: -1: 1$ # Initial to Terminal Conditions	
5		do:	Recompute, H in accordance of 3.12 # Riccati Recurrence
6			Recompute K in accordance of 3.13 # Optimal DLQR Gain
7	**End:**	Computation	

Now, the closed-loop state matrix of A_{cl} is solved by applying the solution of equation 3.15 by using the equation 3.13. The result of A_{cl} is given in equation 3.16.

$$A_{cl} = \begin{bmatrix} 0.2751 & -0.1194 & 0.0183 \\ 2 & 0 & 0 \\ 0 & 1 & 0 \end{bmatrix} \ldots\ldots\ldots (3.16)$$

Finally, the discrete-time closed-loop transfer function is denoted by the following equation of 3.17 as $\mathrm{G_{cl-EHSS}}$. The numerical analysis is presented in accordance of the zero order hold method of calculating the discrete-time transfer function. By holding each sample value of the given input, the ZOH technique achieves an exact match between the continuous-time and discrete-time systems in the time domain for staircase inputs. This method is used in Matlab to convert a continuous-time transfer function to a corresponding discrete-time transfer function by holding each sample value of the given input in the time domain as, $\mathrm{u(t)}$ to obtain the discrete-time representation as $\mathrm{u(k)}$ where, k denotes the sample intervals [37]. The detailed Matlab code to derive the equation 3.17 is included in appendix B.

$$G_{cl-EHSS} = \frac{y(k)}{u(k)} = C(zI - A_{cl})^{-1}B = \frac{0.9536\,z^2 + 3.814z + 0.9536}{z^3 - 0.2751z^2 + 0.2388z - 0.03665} \dots\dots\dots (3.17)$$

3.5 Analysis of Closed-loop Performance of EHSS with DLQR Controller

The closed-loop performance of EHSS coupled with the DLQR based optimal controller is studied by observing the variation in the pole and zero positions over the z-plane obtained from the closed-loop transfer function, expressed in equation 3.17. Firstly, the pole zero plot (PZ plot) is obtained for the discrete-time closed-loop transfer function of EHSS as denoted by $G_{cl-EHSS}$ which is illustrated in Fig. 3.2.

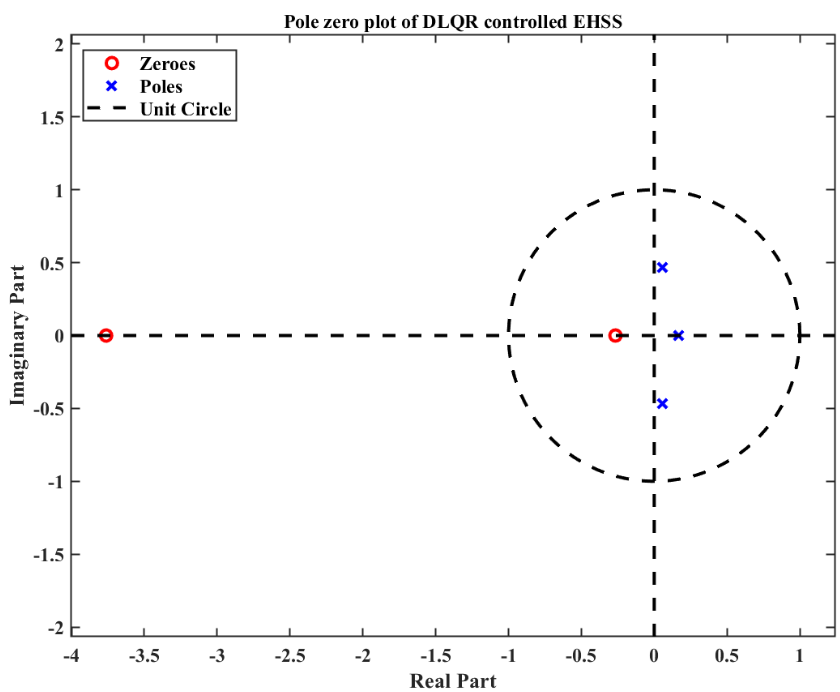

Fig. 3.2 Pole Zero Plot of EHSS with DLQR obtained from the $G_{cl-EHSS}$

The closed-loop PZ plot, as opposed to the open-loop version of the same presented in Fig. 2.3, does demonstrate an improvement in stability of the response. Closed-loop PZ plot results all the poles inside the unit circle on the z-plane, as shown in Fig. 3.2. Moreover, the poles have been pushed further towards the center of the unit circle of the z-plane, improving the relative stability. However, one of the zeroes is still outside of the unit circle, indicating that even after the optimization applied through the DLQR controller, EHSS continues to exhibit NMP behavior to some extent, despite the improvements in the positions of poles since the initial open-loop case.

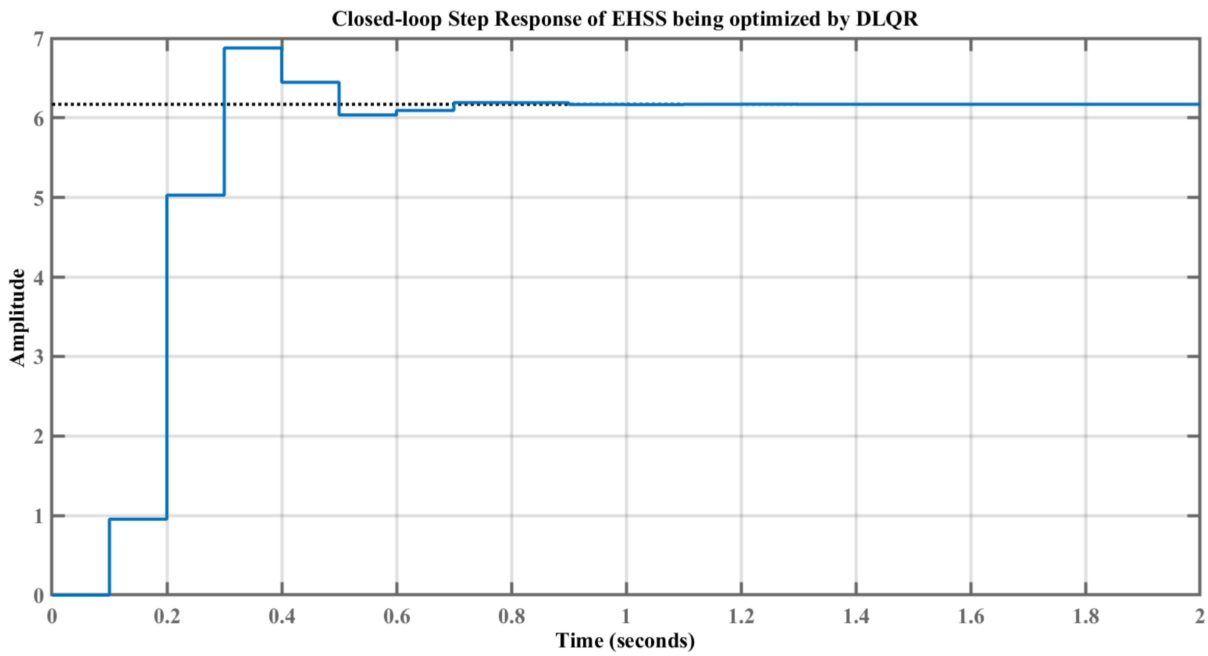

Fig. 3.3 Closed-loop Step Response of EHSS being optimized by DLQR

The closed-loop step response for the EHSS being optimized by the DLQR controlled as derived above, is shown in Fig. 3.3. These illustrations from the numeric analysis by obtaining the PZ plot for both cases of the nature of the spool-valve displacement of the EHSS as a standalone system in comparison to the optimization achieved by applying the DLQR still resonate the insufficiency in the improvement of NMP phenomenon while the relative stability is improved. The same conclusion can be further drawn by analyzing the step response of the closed-loop transfer function of equation 3.17.

Along with the depiction of Close loop PZ Plot and step response as mentioned above, the comparative bode diagrams, showing both of the open-loop and closed-loop cases, also cement that the EHSS being optimized with a DLQR based controller invoking optimal constraints, still exhibits NMP behavior.

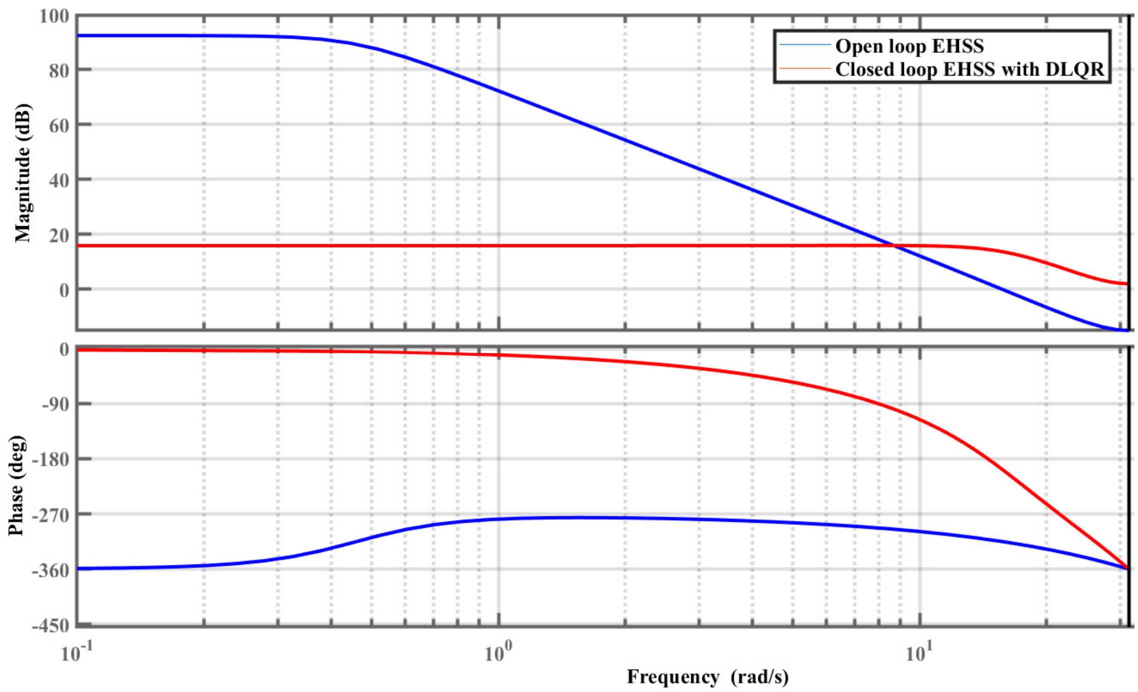

Fig. 3.4 Comparative Bode Diagram of Open-loop and Closed-loop Transfer Functions

The comparative Bode diagram is presented in Fig. 3.4. The blue lines in both of the comparative graphs of Fig. 3.4 show the open-loop phase and amplitude response while the red lines represent the same responses for closed-loop case of this simulation.

In light of these simulated findings, the total performance of the EHSS being optimized by the DLQR-based control may be thoroughly described as: all RHS poles of the z-plane are pushed toward the LHS of the unit circle, therefore improving the stability of the EHSS.

The solitary circle zero that is beyond the unit circle, on the other hand, continues to cause the system's reaction to being NMP. It can be summarized that the EHSS issues must be addressed by developing a mathematical model that incorporates all of the dynamic parameters, including the uncertain load movement that affects the response of the spool-valve as well as the unmodeled disturbances caused by the nature of operation for a system of this type. In the next chapter, EHSS is explained with a comprehensive mathematical model which identifies the parametric uncertainties causing the overall NMP phenomenon in EHSS operation.

Chapter 4

Identification of Parametric Uncertainties for EHSS

4.1 Introduction

Previously, the performance of the electro-hydraulic servo system (EHSS) was analyzed in terms of its nature of non-minimum Phase (NMP) behavior causing the initial dead time to respond while at the same time, the stability of the response was relatively improved. Moreover, these performance dynamics could not be solved explicitly by adopting an optimal control strategy with a feedback gain derived using discrete linear quadratic regulator (DLQR). To some extent, the controller was functional for improving the stability of the system but the NMP behavior was not extinguished completely. On the other hand, the stability was improved after the closed-loop study.

In this chapter, the EHSS is investigated, with static and dynamic performance evaluations of spool-valve displacement subjected to model uncertainties imposed by unknown model parameters, as well as ambient disturbances acting on the load, being carried out under controlled conditions. The results of the simulation reveal a comprehensive mathematical model of the EHSS that includes the parameters that cause the spool-valve displacement to exhibit NMP behavior. The resulting system performances are presented along with the corresponding system performances. Robust control mechanisms to reduce the negative effects of parametric uncertainty are frequently considered as part of a holistic solution in theoretical discussions.

4.2 The Comprehensive Mathematical Model of EHSS

Internal leakage and external load disturbances are taken into account in the mathematical modeling of the EHSS in this chapter. First and foremost, an EHSS is comprised of a hydraulic power supply unit (which includes a torque motor, pump, pressure relief valve, accumulator, filter, and pressure measurement unit and reservoir tank), a double-edged hydraulic cylinder, a servo-valve, a flapper valve working as an amplifier for the servo-valve, a position sensor, and a load. Secondly, the EHSS is comprised of a hydraulic power supply unit which includes changing the input current to the torque motor of the power supply unit, it is intended to achieve its ultimate objective, which is to push the valve position of the cylinder to the desired position as quickly as possible. When the input to the servo controller is applied, the input current produced by the position sensor for the supply torque motor corresponds to the error signal in proportion to the input current generated by the position sensor. Consequently, the input current controls the servo-valve's spool displacement via its spool-valve displacement control. Finally, the cylinders provide hydraulic fuel to the load in response to spool-valve displacement, which varies according to the load circumstances and fluid flow direction.

4.2.1 The Torque Motor

Fig. 4.1 depicts a schematic representation of the orientation of the components of the EHSS. It is essential to construct a mathematical model for each mechanical component of the system in order to get a mathematical model of the whole system. The initial consideration is the torque motor dynamics, which is an electromagnetic component denoted by the symbol as following in the equation 4.1 -

$$T = K_\theta \theta + K_i i_e \ldots\ldots\ldots (4.1)$$

Where, K_θ is the angular rotation-torque gain, θ is the angle of rotation of armature K_i represents the current-torque gain and i_e is the torque motor input current.

The following equation of 4.2 expresses the rotation of motion of the rotating armature of torque motor and associated components [38].

$$T = J\frac{d^2\theta}{dt^2} + f_\theta\frac{d\theta}{dt} + K_T\theta + T_L + T_P + T_F \ldots\ldots\ldots (4.2)$$

Where, J, f_θ, K_T, T_L, T_P, T_F represents the moment of inertia of the rotating components, damping co-efficient, stiffness constant, flapper valve displacement torque, pressure forces torque and feedback torque.

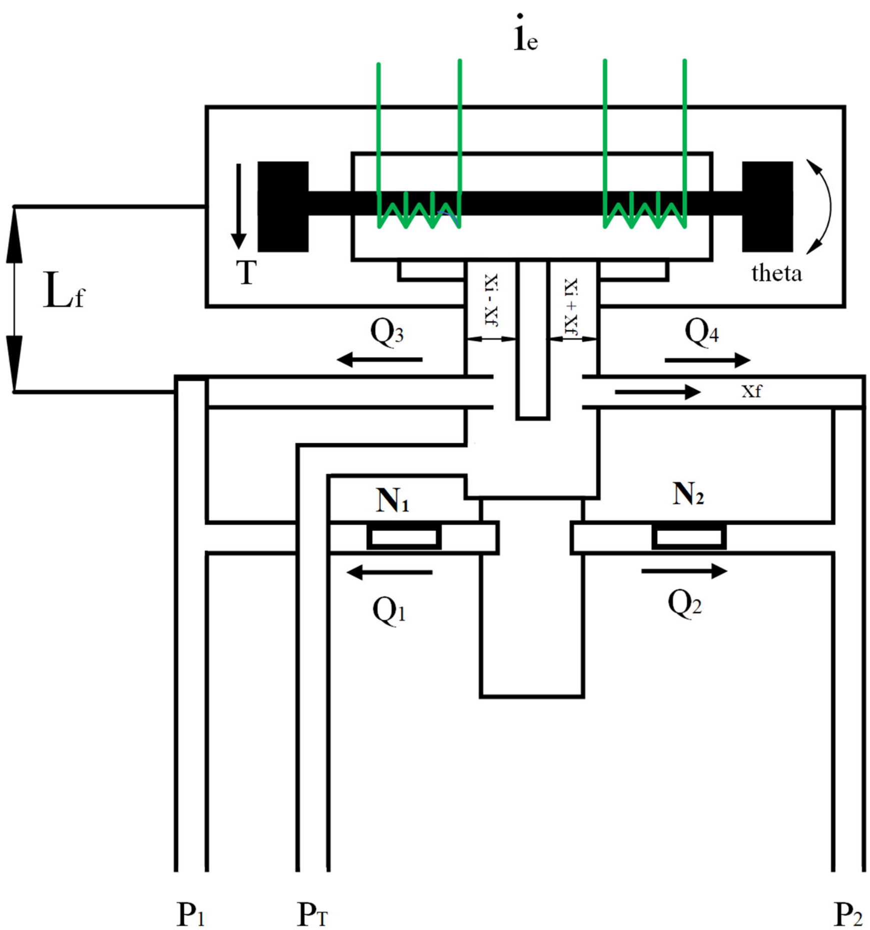

Fig. 4.1 Detailed Schematic Diagram of EHSS

The feedback torque is generated due to the spool displacement of the servo-valve and flapper rotation and it can be mathematically expressed in the equation 4.3.

$$T_F = K_s(L_s\theta + x)L_s \dots\dots\dots (4.3)$$

4.2.2 Hydraulic Fuel Flow Rates

In the equation 4.3, K_s, L_s and x represents, the stiffness of feedback coefficient, length between flapper and spool displacement respectively. Now to obtain the equation of flapper valve displacement torque, it is necessary to obtain the flow rates of hydraulic fluid through the control, supply and the return ports of the flapper.

It is comprised of two fixed ports and two shifting ports for the fluid flow as fluid nozzles. This area of shifting ports is controlled by flapper displacement with supply pressure of fluid denoted as P_s. At normal operating condition, the control ports (control port 1, C_1 and control Port 2, C_2) are closed. The flow rates are denoted by Q_1, Q_2, Q_3, Q_4 where $Q_1 = Q_3$ and $Q_2 = Q_4$ [38].

$$Q_1 = C_D A_0 \left(\frac{2}{\rho}(P_s - P_1)\right)^{1/2} \dots\dots\dots (4.4)$$

$$Q_2 = C_D A_0 \left(\frac{2}{\rho}(P_s - P_2)\right)^{1/2} \dots\dots\dots (4.5)$$

Where the parameters denoted by C_D, A_0, ρ, P_s, P_1 and P_2 are discharge coefficient, port area, fluid density, supply pressure and return port pressure through port C_1. Now, assuming that the total resultant return port pressure as P_T, the fluid nozzles are throttled by separating the flapper opening and fluid nozzles inside the cylinder. Also, assuming that the flapper displacement at the position of fluid nozzle and initial flapper position at the beginning of nozzle opening causing the flapper to be limited in displacement are x_i and x_f respectively along the axis of displacement denoted as "x" in Fig. 4.1, then the rest of the flow rates are expressed mathematically in equation 4.6 and in equations 4.6 to 4.8 where $x_f = L_f\vartheta$ of which L_f is the flapper length and Q_3, Q_4 and Q_5 indicate the left flapper, right flapper and flapper valve drain flow rates respectively.

$$Q_3 = C_d \pi d_f (x_i + x_f)\left(\frac{2}{\rho}(P_1 - P_T)\right)^{1/2} \dots\dots\dots\dots (4.6)$$

$$Q_4 = C_d \pi d_f (x_i - x_f)\left(\frac{2}{\rho}(P_2 - P_T)\right)^{1/2} \dots\dots\dots (4.7)$$

$$Q_5 = C_d A_s\left(\frac{2}{\rho}(P_3 - P_T)\right)^{1/2} = C_5 (P_3 - P_T)^{1/2} \dots\dots\dots (4.8)$$

4.2.3 Pressures of Hydraulic Fluid Flow

As a result, the pressure due to flapper valve displacement produced by the opening and shutting of control ports as a result of the motions described above can now be represented as shown in equation 4.9.

$$P_L = \frac{P_2 - P_1}{P_s} = \frac{4a{x_i}^2}{(1 + a{x_i}^2)} * \frac{x_f}{x_i} \dots\dots\dots (4.9)$$

Where, $a = \left(\frac{C_d \pi\, d_f}{C_D A_0}\right)^2$, C_d and d_f are the discharge coefficient due to flapper position opening and fluid nozzle diameter respectively.

4.2.4 Counter Torque of Load Displacement

Now, using the jet nozzles as a mechanical restriction, the flapper displacement is restricted. When the seat response reaches either of the side nozzles, it produces a counter torque, T_L, which may be calculated using the following equation 4.10 [39].

$$T_L = R\frac{d\theta}{dt} - (|x_f - x_i|) K_{Lf} L_f \operatorname{sgn}(x_f) \dots\dots\dots (4.10)$$

Where, flapper stiffness and flapper damping coefficient are denoted as K_{Lf} and L_f respectively. Now, the motion of the spool-valve is governed by the fact of changes in load conditions. As a result, the torque due to pressure forces, T_P can be obtained from the following equation 4.10 where, P_A, P_B, A_P, m_P, f_P and K_b are the parameters termed as hydraulic cylinder pressure exerted on the load after the resultant flapper displacement, servo-valve piston area, piston mass, piston friction coefficient and load coefficient [40].

$$A_P(P_A - P_B) = m_P \frac{d^2y}{dt^2} + f_P \frac{dy}{dt} + K_b y \dots \dots \dots (4.11)$$

Finally, the torque due to pressure exerted on the cylinder due to changes of load can now be derived as equation 4.12.

$$T_P = \frac{\pi}{4} d_f^2 (P_2 - P_1) L_f \dots \dots \dots (4.12)$$

4.2.5 Spool-valve Displacement

Thus, the spool-valve motion can now be derived as the following equation 4.13.

$$A_s(P_2 - P_1) = m_s \frac{d^2x}{dt^2} + f_s \frac{dx}{dt} + F_j + F_s \dots \dots \dots (4.13)$$

Where, $F_j = \begin{cases} \left(\frac{\rho Q_b^2}{C_c A_b} + \frac{\rho Q_d^2}{C_c A_d}\right) sign(x) \quad while,\ x > 0 \\ \left(\frac{\rho Q_a^2}{C_c A_c} + \frac{\rho Q_c^2}{C_c A_c}\right) sign(x) \quad while,\ x < 0 \end{cases}$ is the hydraulic momentum Force, C_c is the Concentration co-efficient, f_s is the Spool friction co-efficient, m_s is the spool mass and F_s is the applied force at the maximized state of the feedback spring attached to flapper valve. The rate of flows of hydraulic fluid through the restricted area of the flapper valve towards the cylinder housing the spool-valve are given in the following equations from 4.14 to 4.17 where, the valve displacement range with respect to the area of the flapper valve are given in equations 4.18 and 4.19 where c, ω and P_A and P_B indicate the radial clearance of the spool-valve, port widths at the ends of the spool-valve and the pressures exerted on both edges of the hydraulic cylinder, respectively.

$$Q_a = C_d A_a(x)\left(\frac{2}{\rho}(P_A - P_T)\right)^{1/2} \dots\dots\dots\dots (4.14)$$

$$Q_b = C_d A_b(x)\left(\frac{2}{\rho}(P_S - P_A)\right)^{1/2} \dots\dots\dots\dots (4.15)$$

$$Q_c = C_d A_c(x)\left(\frac{2}{\rho}(P_S - P_B)\right)^{1/2} \dots\dots\dots\dots (4.16)$$

$$Q_d = C_d A_d(x)\left(\frac{2}{\rho}(P_B - P_T)\right)^{1/2} \dots\dots\dots\dots (4.17)$$

$$A_a = A_c = \omega c \text{ and } A_b = A_d = \omega(x^2 + c^2)^{1/2} \text{ while } x \geq 0 \dots\dots\dots (4.18)$$

$$A_a = A_c = \omega(x^2 + c^2)^{1/2} \text{ and } A_b = A_d = \omega c \text{ while } x \leq 0 \dots\dots\dots (4.19)$$

It is now possible to derive the continuity equations of flow rates to the cylinder chambers while taking into account the internal leakage given in the following equations from 4.20 to 4.21 where, A_P indicates the piston area, R_i indicates the internal leakage resistance and V_c indicates the half volume of the filling hydraulic fluid.

$$Q_b - Q_a - A_P\frac{dy}{dt} - \frac{P_A - P_B}{R_i} = \frac{V_c + A_p y}{B} \cdot \frac{dP_A}{dt} \dots\dots\dots (4.20)$$

$$Q_c - Q_d - A_P\frac{dy}{dt} + \frac{P_A - P_B}{R_i} = \frac{V_c - A_p y}{B} \cdot \frac{dP_B}{dt} \dots\dots\dots (4.21)$$

The displacement of the piston is detected by a displacement transducer and sent back to the electronic controller, which produces the appropriate error signal based on the displacement and this process of feedback loop is described in the following equation 4.22 where i_e is the Control current, i_b is the Feedback current the K_{FB} indicates the Feedback gain.

$$i_e = i_b - K_{FB}y \ldots\ldots\ldots (4.22)$$

Table 2 Model Parameters for the Comprehensive Mathematical Modeling of EHSS

Parameters of EHSS	**Denoted by**	**Values**	**Unit (SI)**
Current Gain	K_i	0.556	
Armature Damping Ratio Co-efficient	f_{TH}	0.002	
Moment of Inertia of rotor	J	$5x10^{-7}$	Kg-m^2
Flexible Tube rotational stiffness	K_T	10	
Armature rotational stiffness Torque gain	K_{TH}	$9.4x10^{-4}$	
Flapper length	L_f	0.009	m
Mechanical feedback spring length	L_S	0.03	m
Flapper limiting displacement	X_i	$30x10^{-6}$	m
Flapper diameter	d_f	0.0005	m
Equivalent flapper seat material damping coefficient	R_f	5000	N-m^2
Flapper sear equivalent stiffness	K_{LF}	$5x10^{6}$	N/m
Oil density	ρ	867	Kg/m^3
Hydraulic amplifier nozzle diameter	d_{fn}	0.0005	m
Return orifice diameter	d_5	0.0006	m
Spool diameter	d_s	0.00462	M
Initial volume of oil in spool side chamber	V_0	$2x10^{-6}$	m^3
Bulk modulus of oil	β	$1.5x10^{9}$	Pa

Initial Volume of oil in return chamber	V_3	$5x10^{-6}$	m^3
Spool mass	m_S	0.02	Kg
Spool damping coefficient	f_S	2	N/m
Feedback spring stiffness	K_S	900	N/m
Supply Pressure	P_S	$2x10^7$	Pa
Return Pressure	P_T	0	Pa
Servo actuator feedback gain	k_{fb}	3	
Spool port width	ω	0.002	m
Piston area	A_P	$1.25x10^{-3}$	m^2
Initial volume of Hydraulic fluid in cylinder chamber	V_c	$100x10^{-6}$	m^3
Piston mass	m_P	10	kg
Piston loading co-efficient	K_y	0	
Friction coefficient on piston	f_P	1000	

The mathematical models of the entire operation of EHSS as derived above from equations 4.1 to 4.22 can now be utilized to create simulation models using Simulink by applying the numeric values shown in Table 2 for the parameters involved in deriving these equations which are typically observed in electro-hydraulic servo actuators as discussed in section 4.2 [41]. The step response of the systems has been computed as a result of this simulation. Simulation results are discussed in the next section.

4.3 Simulation Results of Comprehensive Mathematical Model of EHSS

The dynamics of EHSS as explained through the mathematical relations of corresponding parameters of distinguished parts of the entire system to result into the movement of the piston in the cylinder as shown in Fig. 4.1 was presented as the displacement of the load attached to it. The load displacement in this manner is caused by the spool-valve displacement due to difference in supply and return pressure of the hydraulic fluid, parameterized as P_1 and P_2 in the previous section, the cylinder is subjected to the force exerted due to this difference in hydraulic fluid pressure on the piston. This sequential mechanical phenomenon is modeled using Simulink environment of the software package of Matlab version 2019a which is a well accepted mathematical modeling simulation platform by the Mathworks Inc [42], [43].

In order to obtain the response of load displacement due to the displacement of the spool-valve, the operation is thus modeled in Simulink as shown in Fig. 4.3.

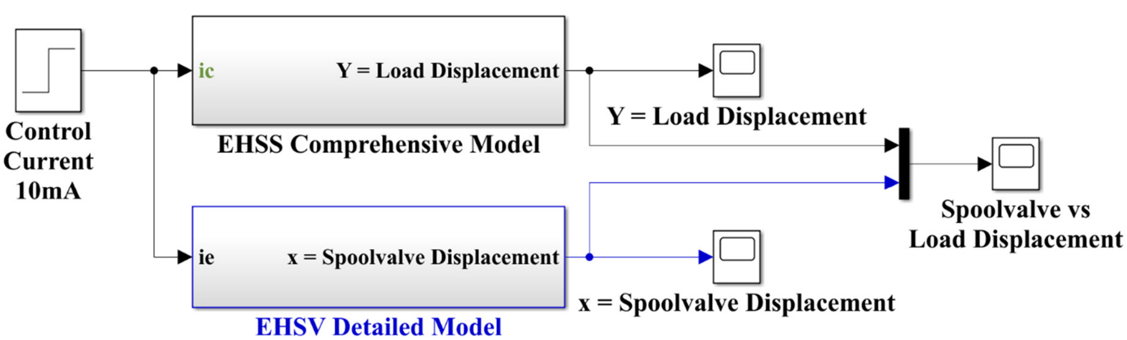

Fig. 4.2 SIMULINK Block Diagram of EHSS Operation

In the Simulink block diagram presented in Fig. 4.3, the electro-hydraulic servo-valve (EHSV) is modeled in accordance with the equations developed for the torque generated by the motor supplying the hydraulic fluid along with the functionals of spool-valve motion due to pressure differences due to differences in flow rates. The EHSV detailed model is shown in Fig. 4.4 while the comprehensive EHSS model inclusive of the cylinder for load displacement is given in Fig. 4.5. Details of these Simulink models are included in Appendix C.

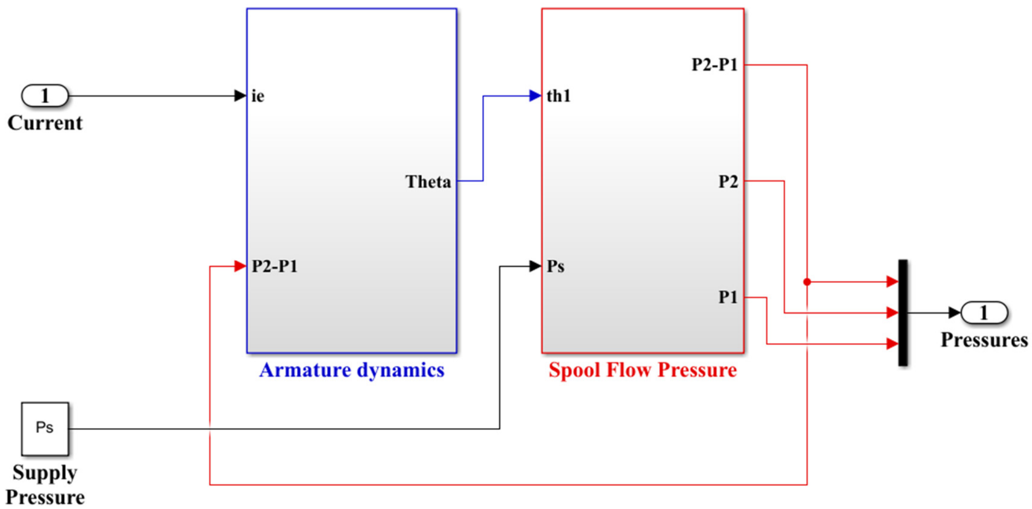

Fig. 4.3 SIMULINK Block Diagram of Supply Pressures for Spool-valve Displacement

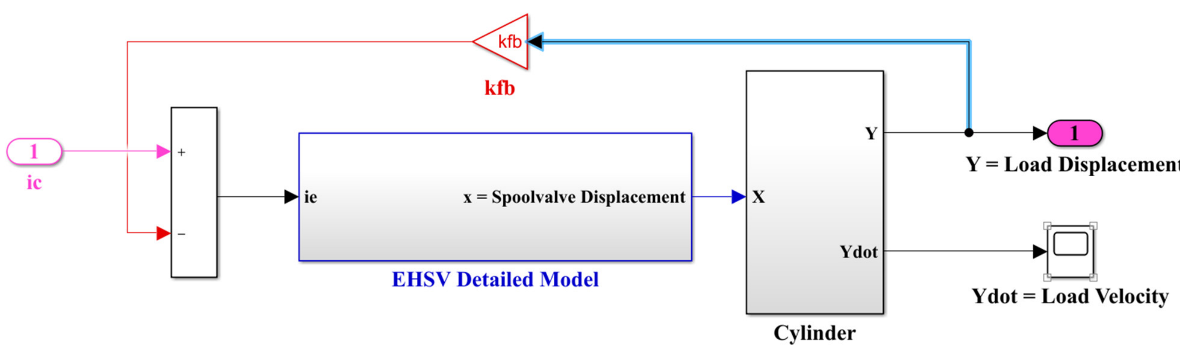

Fig. 4.4 EHSS Comprehensive SIMULINK Block Diagram

All of these simulations for the models depicted as block diagrams from Fig. 4.3 to 4.5 are performed by applying a constant direct current of 10 mA as the control current for 30 ms.

The response of pressures P_1 and P_2 along with the differences are shown in Fig. 4.5 as the initial condition of the operation for the pressures exerted on both sides of the piston remains the same, while the same is shown as initial conditions of flow rates causing the flapper valve displacement as an amplifier for the spool-valve in Fig. 4.6.

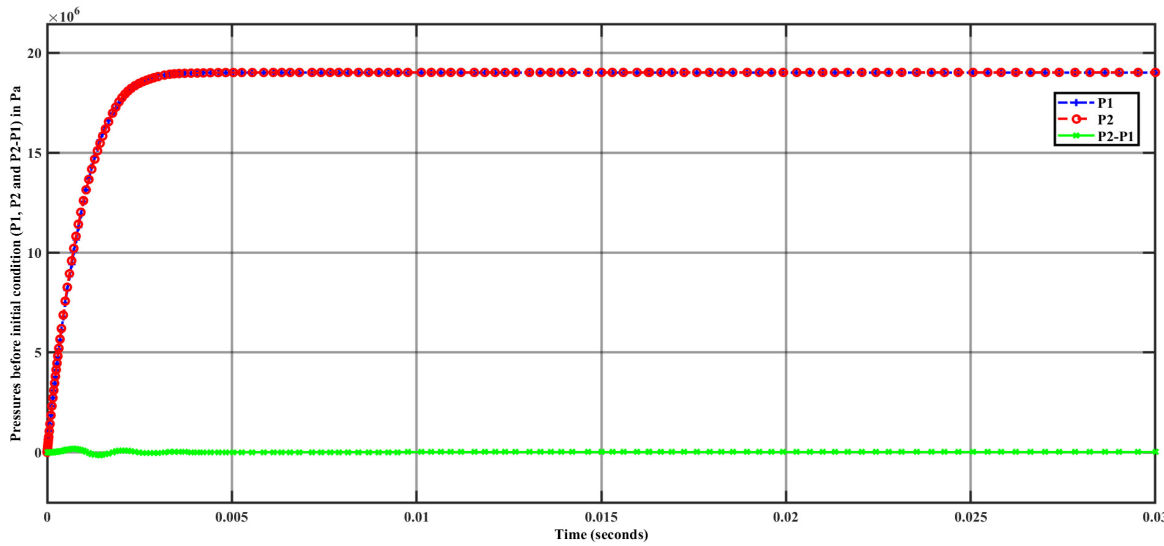

Fig. 4.5 Pressure dynamics before initial conditions are applied

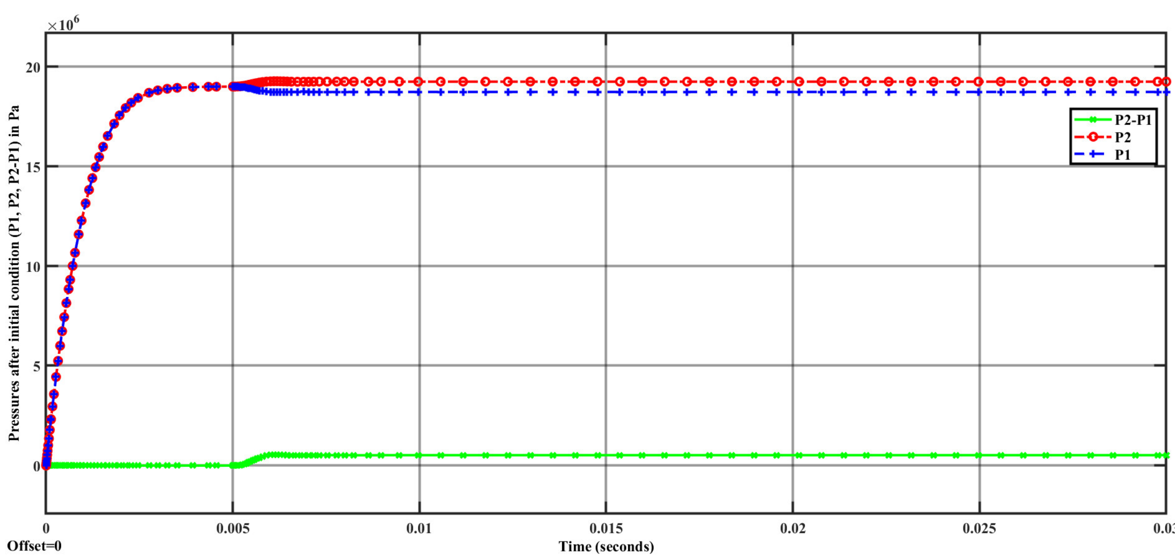

Fig. 4.6 Pressure Dynamics after the initial conditions are applied

The response of spool-valve displacement caused by these pressure dynamics is illustrated in Fig. 4.7 and the corresponding load displacement is present in Fig. 4.8.

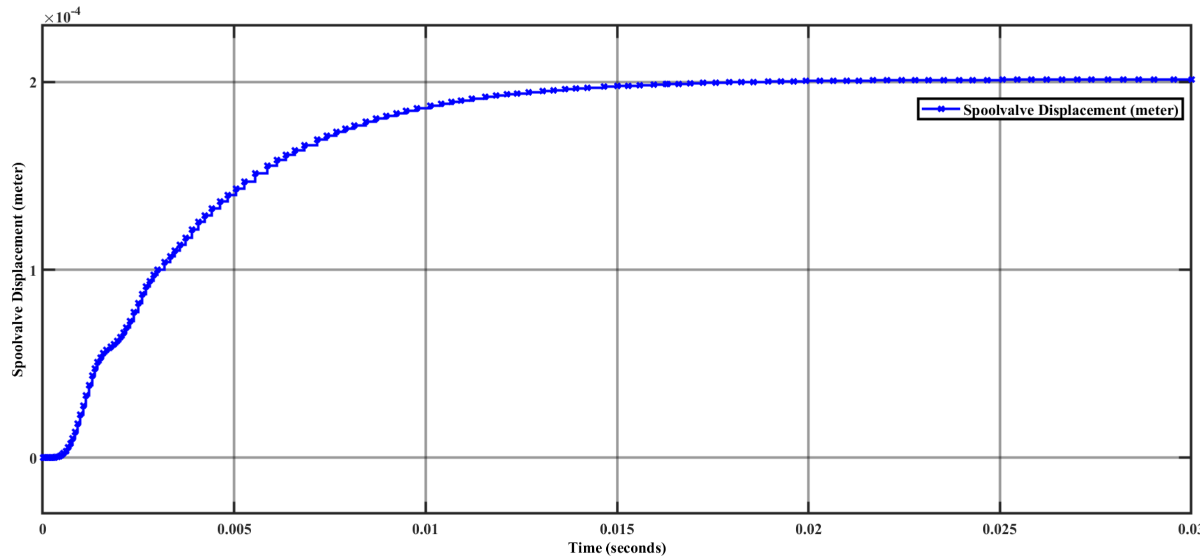

Fig. 4.7 Response of Spool-valve Displacement

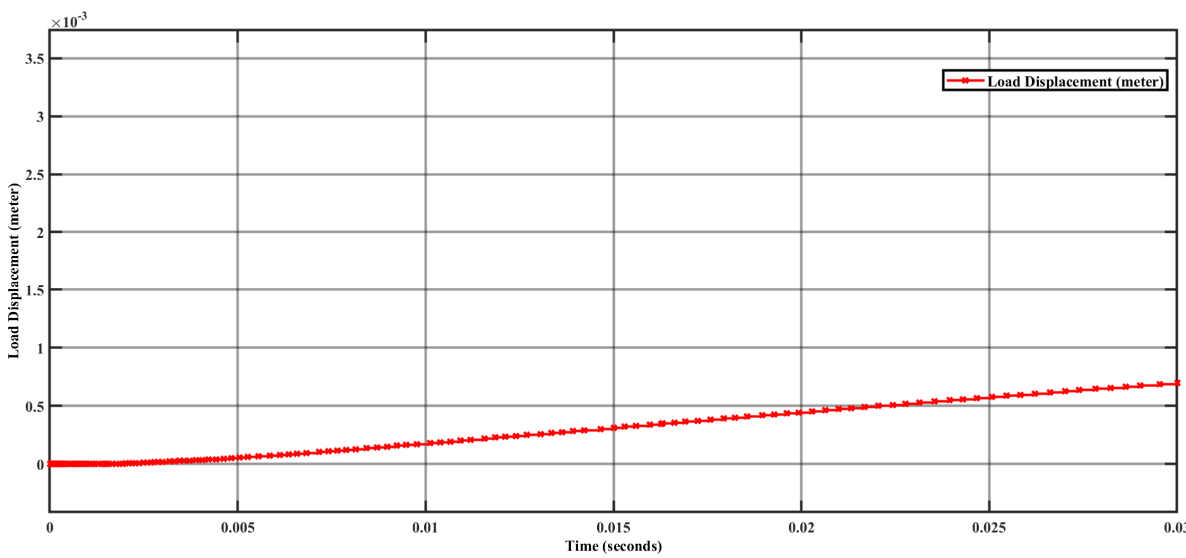

Fig. 4.8 Response of Load Displacement

To understand the delay in response caused by the NMP behavior of EHSS, a comparative analysis of the load displacement with respect to the spool-valve displacement is presented in Fig. 4.9.

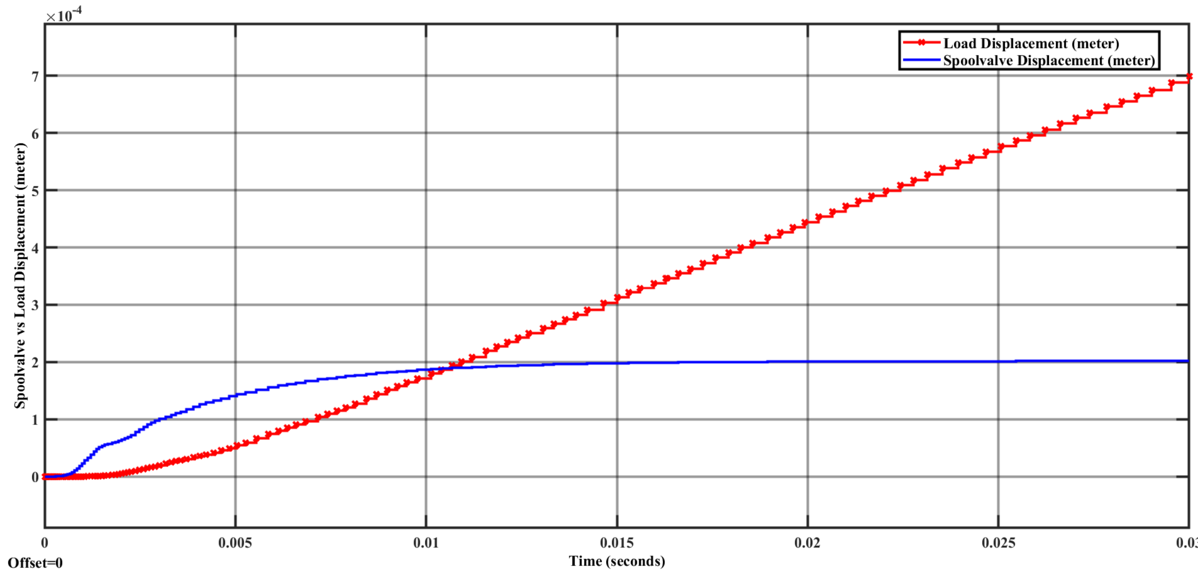

Fig. 4.9 Load vs Spool-valve Displacement for the first 30 ms

It is seen that the settling time for load displacement gets further delayed than the settling time of the Spool-valve displacement response which results into the dead time responsible for NMP behavior. This phenomenon is further illustrated by the comparative analysis of both of these responses in the first 30 ms for the same 10 mA control excitation. Corresponding load velocity response due to the piston movement in the cylinder is also given in Fig. 4.10.

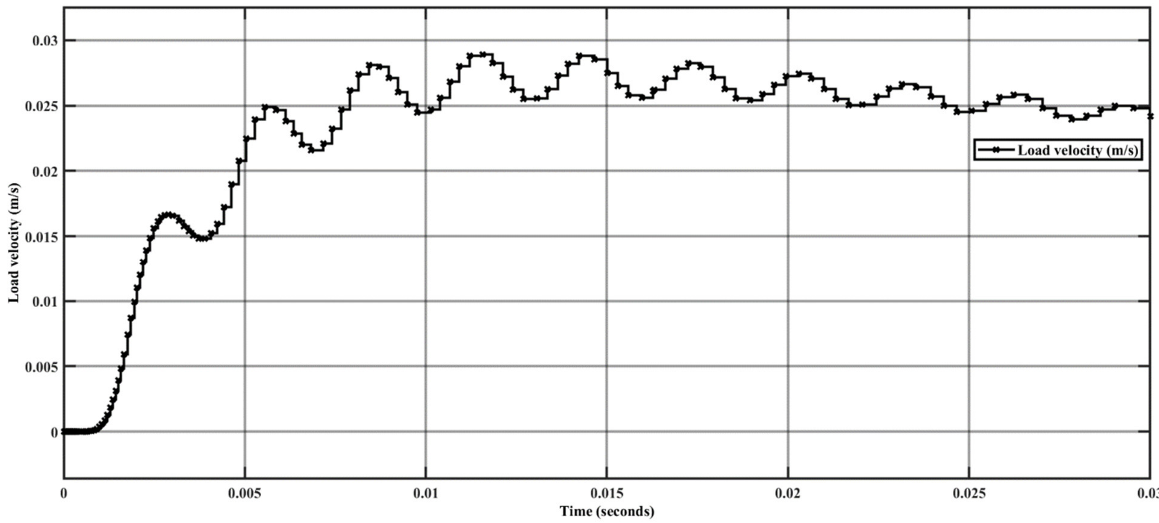

Fig. 4.10 Load velocity response

The simulation results of the comprehensive mathematical model of the EHSS where the internal leakages of hydraulic fluid are taken into account with functional each system component in accordance of respective excitation and response also resonate the existence of inherent stability problems coupled with NMP properties. Thus, it is necessary to identify the specific parameters causing the system to behave in these manners to adopt a complete control strategy to denounce all the operational obstacles. Parametric uncertainties are thus explained in details in the next section.

4.4 Parametric Uncertainties of EHSS

To be able to identify the parameters contributing to the performance uncertainties of EHSS in responding to drive the load, associated mechanical components and systems are required to be identified as well. Fig. 4.11 shows those elements with denotations with the schematic diagram of the EHSS consisting of the piston and the load.

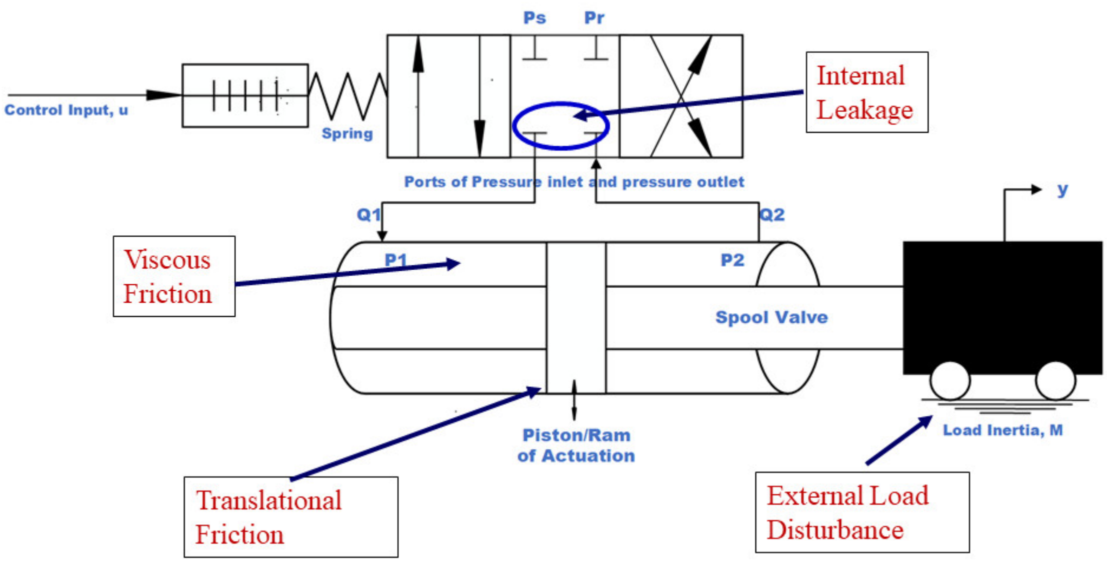

Fig. 4.11 EHSS Schematic with Mechanical Components contributing to the Performance Uncertainties

In Fig. 4.11, P_s and P_r represent the supply and return pressures of the hydraulic fluid powered by the torque motor, respectively, while Q_1 and Q_2 represent the supply and return rates of flow of the hydraulic fluid that generates the pressure differential on the spool-valve, respectively. The intake and exit ports are subjected to pressures denoted by the letters P_1 and P_2, respectively. The difference between these two pressure values causes the force on the spool-valve to displace the piston connected to it, which in turn causes the associated mass-damper load to be driven. During operation, however, the load is exposed to a variety of unpredictable environmental disturbances.

This external load disturbance has an influence on the operation of the piston movement, which, in turn, has an effect on the spool-valve operation as well. The pressures exerted by the hydraulic fluid, on the other hand, are in a state of constant viscous friction while being fed from the hydraulic fuel tank and ending up in the cylinder chamber.

Additionally, the translational friction is produced in the same operational range for both the mechanical displacements of the spool-valve and the piston in conjunction with this. The supply and return ports are also responsible for any possible internal leakages that may occur during the passage of hydraulic fluid through the system. This is accomplished by using all of the characteristics to describe the complete motion dynamics. as equation 4.23 [44].

$$M\ddot{y} = P_1A_1 - P_2A_2 - B\dot{y} - A_fS_f(\dot{y}) - f(y, \dot{y}, t) \ldots \ldots \ldots (4.23)$$

where,

a) $M\ddot{y}$ is the load movement torque due to displacement of spool-valve while M is the load inertia and y is the angular displacement of the load.

b) $P_1A_1 - P_2A_2 = u(t)$ is the resultant input force due to the difference in supply and return pressure inside the cylinder.

c) $B\dot{y}$ is the loss due to viscous friction force caused by the flow of hydraulic fluid inside the cylinder where B represents the viscous co-efficient of hydraulic fluid.

d) $A_fS_f(\dot{y})$ is the loss due to translational friction force incurred by the piston movement inside servo actuator cylinder where A_fS_f is the representation of non-linear Coulomb friction [45]. Here, the quantity of A_f indicates the amplitude of translational friction force while S_f is the continuous shape function of the translational body.

e) $f(y, \dot{y}, t)$ is the external disturbances being caused by the nonlinearities of the unmodeled parameters. These are lumped together since they cannot be accurately described with precision [46].

Now, if any external leakages of the servo mechanism consisting of the cylinder and the spool-valve are ignored, the kinetics of pressures inside the cylinder can be expressed as given in the equation 4.24.

$$\left.\begin{aligned} \dot{P}_1 &= \frac{\beta_e}{V_{01} + A_1 y}\left[-A_1\dot{y} - C_t P_L + Q_1\right] \\ \dot{P}_2 &= \frac{\beta_e}{V_{02} + A_2 y}\left[A_2\dot{y} + C_t P_L - Q_2\right] \end{aligned}\right\} \ldots\ldots\ldots (4.24)$$

Where, β_e is the effective bulk modulus of the hydraulic fluid while V_{01} and V_{02} are the initial volumes of the two chambers of the cylinder separated by the piston for inlet and outlet of the hydraulic fluid, respectively. C_t is the co-efficient of the total internal leakage inside the cylinder with the piston area and P_L is the difference of pressures P_2 and P_1 as explained earlier. Associated with the displacement of the spool-valve, Q_1 and Q_2 are the inlet and outlet flow rates, respectively, which in extent are formulated as equation 4.25 [47].

$$\left.\begin{aligned} Q_1 &= k_q x_v\left[s(x_v)\sqrt{P_s - P_1} + s(-x_v)\sqrt{P_1 - P_r}\right] \\ Q_2 &= k_q x_v\left[s(x_v)\sqrt{P_2 - P_r} + s(-x_v)\sqrt{P_s - P_2}\right] \end{aligned}\right\} \ldots\ldots\ldots (4.25)$$

Where, $k_q = C_d w\sqrt{\frac{2}{\rho}}$ is the gain of discharge due to the Spool-valve displacement involving C_d as the discharge co-efficient, ρ is the hydraulic fluid density and w as the spool-valve area gradient. On the other hand, x_v is the spool-valve displacement and $s(x_v)$ is the factor of displacement in regard of unmodeled dynamics of the external disturbances exerted backward from the load on the spool-valve of the following constraints as shown in equation 4.26 which also supposes that the actuation exerted by the cylinder to drive the load exactly proportional to the spool-valve position such that $s(x_v) = s(u)$ while $x_v = k_i u(t)$ [48]. k_i is the electric constant of the supplied current into the torque motor.

$$s(x_v) = \begin{cases} 1, & for\ x_v \geq 0 \\ 0, & for\ x_v < 0 \end{cases} \quad \dots\dots\dots (4.26)$$

Hence, equation 4.25 can be simplified as equation 4.27.

$$\left.\begin{array}{r} Q_1 = GZ_1 u \\ Q_2 = GZ_2 u \end{array}\right\} \dots\dots\dots (4.27)$$

Where, $Z_1 = s(u)\sqrt{P_s - P_1} + s(-u)\sqrt{P_1 - P_r}$ and $Z_2 = s(u)\sqrt{P_2 - P_r} + s(-u)\sqrt{P_s - P_2}$ and, $G = k_q k_i$ is the flow rate co-efficient.

In practice, hydraulic systems at normal operating conditions tend to be guided by the following assumption I which relates the supply and return pressure of the hydraulic fluid with the pressures wielded on the cylinder for piston displacement [49].

Assumption I:

a) $0 < P_r < P_1 < P_s$

b) $0 < P_r < P_2 < P_s$

As a result, the motion dynamics of EHSS with parametric uncertainties posed by the constraints of internal leakage and external load disturbance as explain through the equations from 4.23 to 4.27, can now be expressed as a state space model as given in equation 4.28 by defining $x = \begin{bmatrix} x_1 \\ x_2 \\ x_3 \end{bmatrix} = \begin{bmatrix} y \\ \dot{y} \\ A_1 P_1 - A_2 P_2 \end{bmatrix}$

$$\left.\begin{aligned} \dot{x_1} &= x_2 \\ M\dot{x_2} &= x_3 - Bx_2 - A_f S_f(x_2) - d_n - d(x_1, x_2, t) \\ \dot{x_3} &= \left(\frac{A_1}{V_1}Z_1 + \frac{A_2}{V_2}Z_2\right)G\beta_e u - \left(\frac{A_1^2}{V_1} + \frac{A_2^2}{V_2}\right)\beta_e x_2 - \left(\frac{A_1}{V_1} + \frac{A_2}{V_2}\right)\beta_e C_t P_L \end{aligned}\right\} \dots\dots\dots (4.28)$$

Where, d_n is the nominal accumulated quantity of the unmodeled dynamics being related to the external load disturbances such that, $d_n = f(x_1, x_2, t) - d(x_1, x_2, t)$ [50]. Here, $d(x_1, x_2, t)$ is the unstructured uncertainties of the system which is impossible to be expressed as a function, explicitly.

Because of the significant fluctuations in system parameters, the system is exposed to structural uncertainties attributed by the parameters listed in the Table 3.

Table 3 Unmodeled Parameters for Model Uncertainties of EHSS

Parameters	**Denoted by -**
Mass of the Load	M
Viscous Friction Co-efficient	B
Amplitude of the Translational Friction	A_f
Volume of the inlet pressure part of the Cylinder before the displacement of the piston	V_{01}
Volume of the outlet pressure part of the Cylinder before the displacement of the piston	V_{02}
Flow rate co-efficient	G
Oil Bulk Modulus of the Hydraulic Fluid	β_e
Co-efficient of the total Internal Leakage	C_t

Considering with assumption that the parameters – B, A_f, d_n and C_t are impossible to be stated, unequivocally, are being regarded as the uncertain parameters inclusive of internal leakage and load disturbance while the other parameters as expressed in Table 3 are all known, these are now being defined as unmodeled yet constant parameter set as of equation 4.29. Additionally, the equation 4.28 is then transformed as shown in equation 4.30.

$$\varphi = \begin{bmatrix} \varphi_1 \\ \varphi_2 \\ \varphi_3 \\ \varphi_4 \end{bmatrix} = \begin{bmatrix} B \\ A_f \\ d_n \\ C_t \end{bmatrix} \quad \dots\dots\dots (4.29)$$

$$\left.\begin{aligned} \dot{x_1} &= x_2 \\ \dot{x_2} &= \frac{1}{M}x_3 - \frac{1}{M}\varphi_1 x_2 - \frac{1}{M}\varphi_2 S_f(x_2) - \frac{1}{M}\varphi_3 - \frac{1}{M}d \\ \dot{x_3} &= G_3 u - F_c x_2 - F_u \varphi_4 \end{aligned}\right\} \dots\dots\dots (4.30)$$

Where, $\left(\frac{A_1}{V_1}R_1 + \frac{A_2}{V_2}R_2\right) G\beta_e = G_3$, $\left(\frac{A_1^2}{V_1} + \frac{A_2^2}{V_2}\right)\beta_e = F_c$ and $\left(\frac{A_1}{V_1} + \frac{A_2}{V_2}\right)\beta_e P_L = F_u$

For the system response to be actuated, a specific set of criterions are required to be met in order to devise a control technique which in turns offset the interference of these parametric uncertainties. Those set of rules are specified in assumption II and assumption III for actively rejecting the impact of unmodeled parameters as incorporated in equation 4.30 resulting in load displacement, accordingly [51].

Assumption II: Parametric uncertainties φ and disturbances d must satisfy -

a) $\varphi \in \gamma_\varphi = \{\varphi : \varphi_{min} \leq \varphi \leq \varphi_{max}\}$

where, $\varphi_{min} = \begin{bmatrix} \varphi_{1min} \\ \varphi_{2min} \\ \varphi_{3min} \\ \varphi_{4min} \end{bmatrix}$ and $\varphi_{max} = \begin{bmatrix} \varphi_{1max} \\ \varphi_{2max} \\ \varphi_{3max} \\ \varphi_{4max} \end{bmatrix}$

b) $|d(x_1, x_2, t)| \leq \alpha_d$ where, α_d is a known function to wield the system response of $y(t)$ such that it remains continuous and bounded.

From the discussion in section 1.2, it is understood that systems with unmodeled parametric uncertainties are difficult to be characterized by a specific controller as it is also evident from the results analyzed in section 3.5 that optimal feedback control technique is inefficient in resolving the stability performance although the system was modeled with known parameters.

In the Table 3, parametric uncertainties induced by changes in physical characteristics of the hydraulic system are represented as unmodeled parameters for model uncertainties of EHSS. The uncertain parameters are represented as unmodeled parameters for model uncertainties of EHSS in the Table 3. As a consequence of these understandings, it is apparent that a disturbance rejection technique through robust control strategy is more suitable for improving the stability criterions of EHSS which is discussed in the next section.

4.5 Active Disturbance Rejection through Robust Control Strategy

The goal of control strategy is to ensure that the inertia load is capable of withstanding disturbances within a certain frequency domain while also stabilizing the system in the presence of external disturbances and system parameter uncertainties. Taking into account, the parametric uncertainties induced by changes in physical characteristics of the hydraulic system, the uncertain parameters may be expressed as follows in equation 4.31 by defining the estimated nominal co-efficient from assumption II (a) [52].

$$\begin{bmatrix} \gamma_{\varphi_1} \\ \gamma_{\varphi_2} \\ \gamma_{\varphi_3} \\ \gamma_{\varphi_4} \end{bmatrix} = \begin{bmatrix} 1 + \varphi_{1\max}\,\delta_{\varphi_1} \\ 1 + \varphi_{2\max}\,\delta_{\varphi_2} \\ 1 + \varphi_{3\max}\,\delta_{\varphi_3} \\ 1 + \varphi_{4\max}\,\delta_{\varphi_4} \end{bmatrix} \ldots\ldots\ldots (4.31)$$

Here, $\delta = \begin{bmatrix} \delta_{\varphi_1} \\ \delta_{\varphi_2} \\ \delta_{\varphi_3} \\ \delta_{\varphi_4} \end{bmatrix}$ is the relative random variation due to uncertain conditions

while $-1 \leq \delta \leq 1$.

The nominal disturbance is similarly represented as shown in equation 4.32.

$$\omega = \begin{bmatrix} \delta_{\varphi_1} x_2 \\ \delta_{\varphi_2} S_f(x_2) \\ \delta_{\varphi_3} \\ \delta_{\varphi_4} \\ \alpha_d \end{bmatrix} \ldots\ldots\ldots (4.32)$$

Thus, the controller based on finite frequency H∞ control method can be designed by calculation of a full-state feedback gain K_H.

$$u(t) = K_H x(t) = \begin{bmatrix} K_{H_1} & K_{H_2} & K_{H_3} \end{bmatrix} \begin{bmatrix} x_1 \\ x_2 \\ x_3 \end{bmatrix} \dots \dots \dots (4.33)$$

In accordance of the linear form of the EHSS the equation of state space model can then be represented as given in equation 4.34.

$$\dot{x} = Ax + Bu + B_1\omega \dots \dots \dots (4.34)$$

The performance requirement for actuating robustness in the response of EHSS dealing with disturbances with more accuracy, the controller output is required to be adjusted as presented in equation 4.35 which, therefore, lead to obtaining equation 4.34 as equation 4.36 concerning the response function of y.

$$z = \begin{bmatrix} x_1 & x_2 & 0 \end{bmatrix} \dots \dots \dots (4.35)$$

$$\left.\begin{aligned} z &= C_1 x \\ y &= C_2 x \end{aligned}\right\} \dots \dots \dots (4.36)$$

Where, $C_1 = \begin{bmatrix} 1 & 0 & 0 \\ 0 & 1 & 0 \\ 0 & 0 & 0 \end{bmatrix}$ and $C_2 = \begin{bmatrix} 1 & 0 & 0 \end{bmatrix}$ which leads to the simplified version of equation 4.34 as equation 4.37 given below [53].

$$\left.\begin{aligned} \begin{bmatrix} \bar{A} & \bar{B} \\ \bar{C} & \bar{D} \end{bmatrix} &= \begin{bmatrix} A + BK_H & B_1 \\ C_1 & 0 \end{bmatrix} \\ \dot{x} &= \bar{A}x + \overline{B_1}\omega \\ z &= \bar{C}x \\ y &= C_2 x \end{aligned}\right\} \dots \dots \dots (4.37)$$

As a result, the controller invoking robust strategy is defined as transfer function, G(jω) where the control objective is to ensure the relation depicted in equation 4.38 which in case of disturbance will suppress the effect on load displacement of EHSS by invoking finite range of operational frequencies denoted as $\overline{\omega_1}$ and $\overline{\omega_2}$ being the upper band and the lower band of the frequency domain, respectively while keeping the response under a prescribed scalar, denoted as σ [54].

$$\sup_{\overline{\omega_1} \leq \omega \leq \overline{\omega_2}} ||\mathrm{G}(\mathrm{j}\omega)||_{\infty} < \sigma \ldots\ldots\ldots (4.38)$$

Thus, the disturbance of the electro-hydraulic servo system (EHSS) within a certain frequency range, taking into consideration all parameter uncertainties is evaluated and a finite frequency H∞ controller is theoretically developed to resolve the problems for achieving gradual stability.

4.6 Computer Simulation for Robust Controller Design

For obtaining the computer simulated numeric results for the above-mentioned control technique, Matlab version 2021a includes the robust control toolbox, which includes functions and blocks for evaluating and adjusting control systems for performance and robustness in the face of plant uncertainty and active disturbance for such systems as described in section 4.2 [55]. When nominal dynamics and uncertain elements, such as uncertain parameters or unmodeled dynamics, are combined mathematically, uncertain models can be analyzed to observe the impact of plant model uncertainty on control system performance, and worst-case combinations of uncertain elements can be identified by applying the H-infinity robust control strategy to design controllers that maximize robustness [56].

4.6.1 Modeling the Effect of Road Disturbance on the Active Suspension

Thus, the load of EHSS which was expressed as the mathematical model without any model uncertainty, can now be represented as shown in Fig. 4.13 for the same system mathematical model, expressed in equation 2.15. As a result, the system is considered to be subjected to the load disturbance employed by the active suspension as given in equation 4.39

as the state-space model, where the denoted suspension parameters are listed in Table 4 which are typically chosen for mathematical modeling of conventional active suspension system [57].

$$\begin{bmatrix} \dot{x_1} \\ \dot{x_2} \\ \dot{x_3} \\ \dot{x_4} \end{bmatrix} = \begin{bmatrix} x_2 \\ -\frac{1}{M_b}[Q_s(x_1 - x_3) + B_s(x_2 - x_4) - 10^3 F_s] \\ \dot{x_4} \\ \frac{1}{M_w}[Q_s(x_1 - x_3) + B_s(x_2 - x_4) - Q_t(x_3 - r) - 10^3 F_s] \end{bmatrix} \dots\dots\dots (4.39)$$

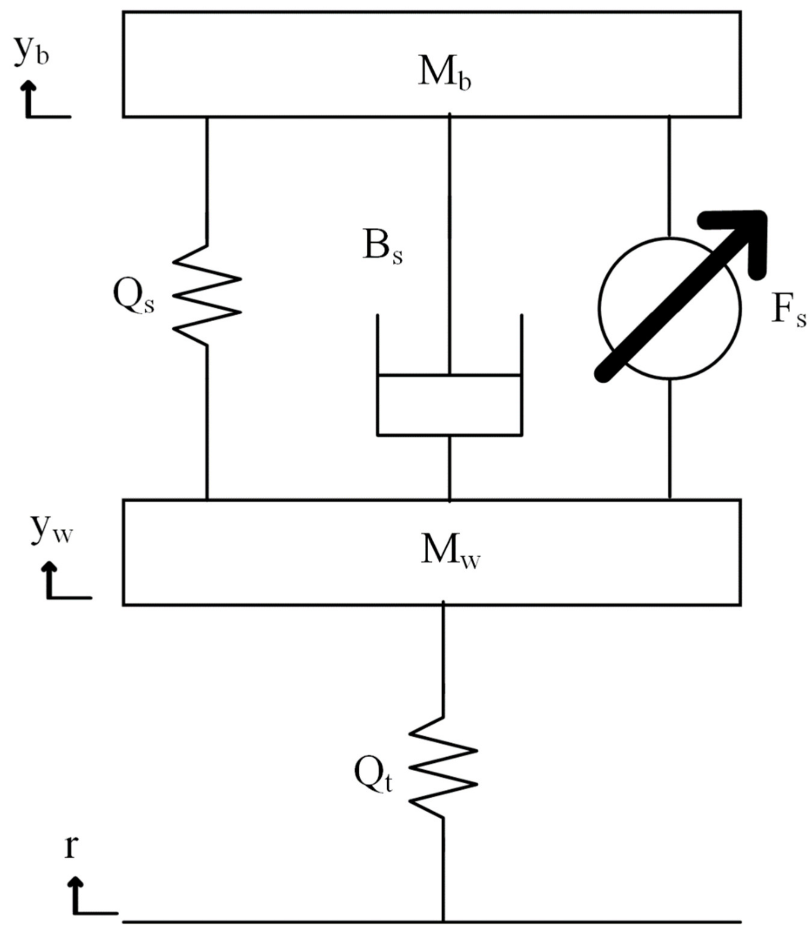

Fig. 4.12 Active suspension model as the load for EHSS without model uncertainties

Table 4 Active Suspension System Parameters for the Modeling

Parameter Type	Parameter Symbol	Numeric Value	Unit
Mass of attached Car-body to the EHSS Active Suspension System	M_b	300	Kg
Mass of the Wheel Assembly for the EHSS Active Suspension System	M_w	60	Kg
Mechanical Spring co-efficient of the Suspension Attached between body and wheel assembly	Q_s	16000	N/m
Compressibility co-efficient of the Wheel due to disturbance exerted by the road	Q_t	19000	N/m
Mechanical Spring Shock Absorber	B_s	1000	N/ms^{-1}

Along with the parameters shown in Table 4, the actuator force between the car-body and the wheel attached with the active suspension due to road disturbances, is denoted by "F_s" while, "y_b" and "y_w" are the displacements of car-body and the wheel attached to suspension due to road disturbance, respectively. The relation between y_b and y_w is given as $y_w = y_b - s_d$, where, s_d is the displacement of suspension to overcome the road disturbance. All these parameters are measured in meter. Meanwhile, the road disturbance, as denoted by "r" in Fig. 4.12 has an impact on the motion of the car's body and the active suspension that is connected to it, resulting in the exertion of oscillating vibration throughout the body's length. In order to reduce the amount of oscillating vibration produced by road disturbance, the suspension displacement must be able to restrict the displacement of the EHSS actuator to ensure riding comfort. The state space model of the active suspension connected to the vehicle body is examined in order to calculate the natural frequency of the disturbance inflicted on the actuator, which is represented by "φ_n" and is known as the "Natural Frequency of Actuation”. In a similar manner, the "Deflection Frequency" of the suspension displacement is calculated and represented by "φ_d" . These calculations are achieved by calculating the zeroes of the transfer function from the actuator to the car-body displacement and the zeroes of the transfer function from the actuator to the suspension displacement. In equation 4.40, the numerical results of the φ_n and φ_d variables are provided.

$$\left.\begin{aligned} \varphi_n &= \begin{cases} -0.0000 + 56.2731i \\ -0.0000 - 56.2731i \end{cases} \\ \varphi_d &= \begin{cases} 0.0000 + 22.9734i \\ 0.0000 - 22.9734i \end{cases} \end{aligned}\right\} \dots\dots\dots (4.40)$$

As evident from equation 4.40, with the imaginary axis zeroes, optimal feedback control can not minimize the effect of oscillating vibration caused by the road disturbances on the body displacement at the natural frequency of actuation as well as at deflection frequency. As a result, body displacement results into small amount of body acceleration, expressed as "a_b".

The gains of road disturbance and the actuator force against the body acceleration and suspension displacement obtained from Matlab simulation for the oscillating vibrations caused by the actuation frequency and deflection frequency are shown in Fig. 4.13.

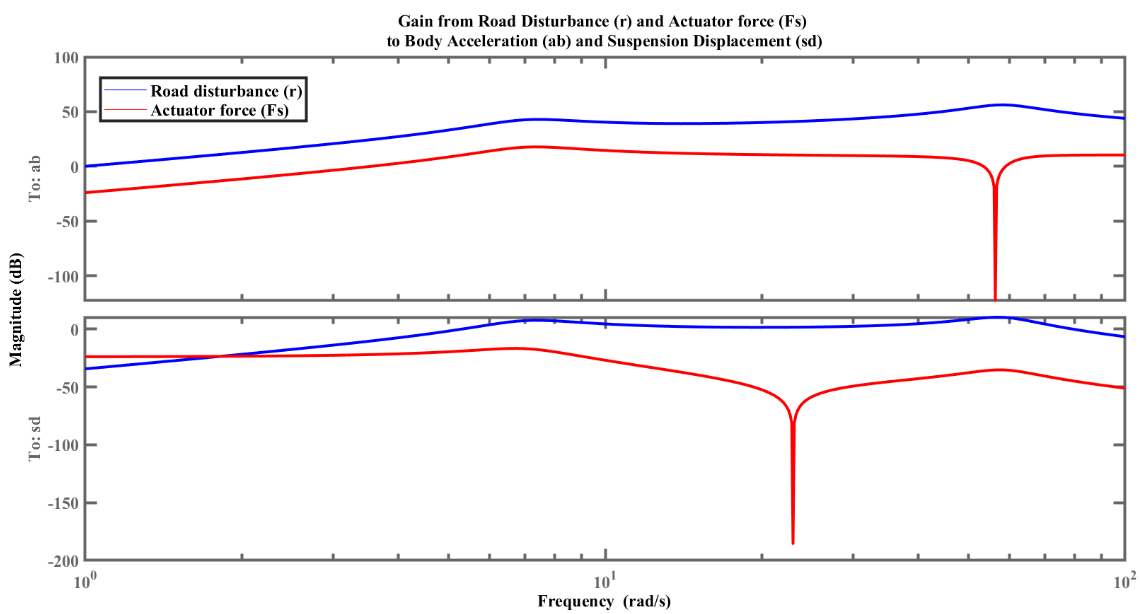

Fig. 4.13 Bode Diagram of Road Disturbance Gain and Actuator Force against Body Acceleration and Suspension Displacement

At low frequency, as shown in Fig. 4.13, the wheel displacement associated with the suspension displacement follows the road disturbance gain in a nearly linear fashion. In addition, there is an intrinsic trade-off between the displacement of the body and the displacement of the suspension. Therefore, any decrease in body displacement at a low frequency will result in an increase in suspension displacement as a consequence of the body displacement reduction.

4.6.2 Parametric Constraint for the Actuator

The actuator of the EHSS deployed for the operation of active suspension as modeled above in the presence of road disturbance is connected to the mass of attached car-body to the EHSS active suspension system and to the mass of the wheel assembly for the EHSS active suspension system. To approximate the simulated response of such actuator dynamics, a nominal actuator model of first order is assumed as $\frac{1}{1+\frac{s}{60}}$ with the maximum displacement constraint for the actuator to reject the road disturbance is also assumed to be 0.05 meter.

The error in model approximation implied by the actuator constraints at the variations of disturbance for different stages of disturbance occurring frequencies are assumed as given in Table 5.

Table 5 Model Approximation Error for Actuator Constraints

Range of Disturbance Frequency (rad/s)	% Error in Model Approximation
Below 3	40%
Around 3	Close to Nominal Approximation (stable)
At 15	100%
At 1000	2000%

In order to modulate the uncertainty posed by the parametric constraints to model approximation of the nominal actuator as described above, a weighting function, $W_{\text{uncertain}}$ is calculated for the various error percentages as mentioned in Table 5, using Matlab's "ultidyn" function which creates uncertain linear time-invariant object [58].

4.6.3 Disturbance Rejection by Robust H∞ Finite Frequency Controller

Control objective of the robust H∞ finite frequency control method is to formulate the rejection of road disturbance on the body displacement considered in terms of riding comfort by denouncing the effect of oscillating vibrations as indicated by body acceleration, a_b as well as to ensure road handing as quantified by suspension displacement, s_d quality for the active suspension actuation system being driven by the EHSS.

A feedback controller employing the finite frequency H∞ control algorithm measures the quantities of x_1 and x_2 as actuations of suspension displacement s_d and body acceleration a_b to generate the control signal "u" to drive the active suspension system associated with the EHSS actuator. The operation of this disturbance rejection control is shown in Fig. 4.14 as below.

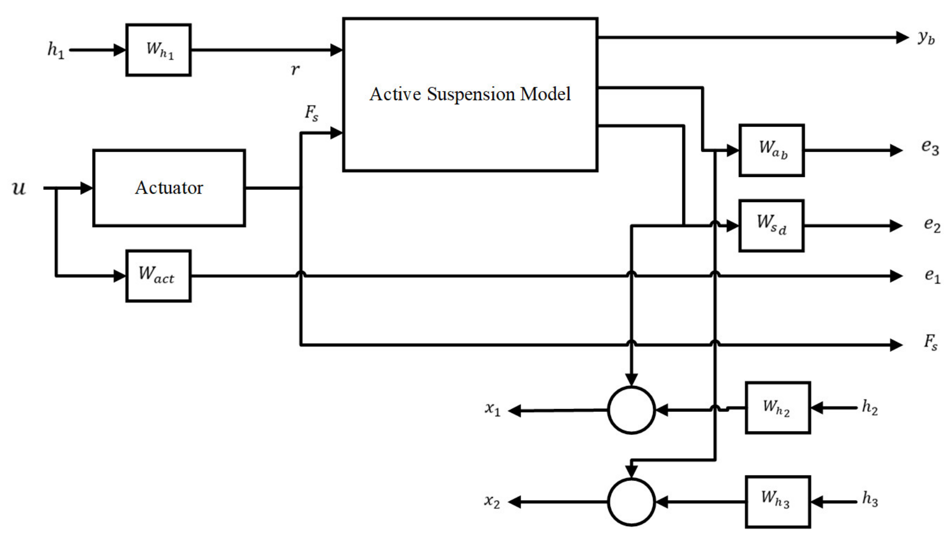

Fig. 4.14 Block Diagram Representation of Robust Control Strategy for the Active Suspension Disturbance Rejection

The presence of external disturbances is categorized as follows –

1. Road Disturbance, u is represented as a normalized signal h_1 being associated with the weighting matrices quantity of uncertainty W_{h_1} and is assumed to be constant in magnitude as, $W_{h_1} = 0.07$.
2. Errors in measurements of body acceleration, a_b and suspension displacement s_d are represented as h_3 and h_2 respectively, being associated with the weighting matrices quantity of uncertainty W_{h_3} and W_{h_2} which are similarly assumed to be quantified as - $W_{h_2} = 0.01$ and $W_{h_3} = 0.5$.

Thus, the control algorithm as shown in Fig. 4.15 can now be interpreted as illustrated in steps of Algorithm 2.

Algorithm 2: Disturbance Rejection Controller			
1	**Initialize:**	Disturbance inputs → $[h_1, h_2, h_3]$ Range of Frequency of Oscillating vibrations in terms of Model Approximation	
2	**Set:**	Model Approximation Uncertainty Weight Matrices– $[W_{h_1}, W_{h_2}, W_{h_3}]$ Initial: Control input as u, Suspension displacement as s_d and Body Acceleration as a_b	
3		%Error of corresponding Approximations – $[e_1, e_2, e_3]$	
4	**While**	%Error < %Error of Model Approximation	
5	**Do:**	Minimize the impact of Disturbance inputs	
6		Recompute %Error → %NewError	
7		If:	%NewError > Model Approximation Apply H∞ Finite Frequency Filter to reduce e_1 Recompute e_2 and e_3 using x_1 and x_2
8		Else:	%NewError → %Error
			Recompute: u, s_d, a_b
9	**End:**	Computation	

The corresponding performance weights, W_{s_d} and W_{a_b} are analyzed in terms of the operational states of the disturbance rejections for all the stated disturbance inputs as discussed in algorithm 2. The rejection criterions are specified as “Soft rejection”, “Balanced rejection” and “Hard rejection” and are denoted by β with numeric assumptions for each type as equation 4.41.

$$[\text{Soft}, \text{Balanced}, \text{Hard}] = [\beta_1, \beta_2, \beta_3] = [0.01, 0.5, 0.99] \dots\dots\dots (4.41)$$

As a result, the performance of H∞ controller to obtain the finite frequency disturbance rejection control is observed through Matlab simulation with corresponding computations for performance level indicator, γ for each criterion of β in equation 4.42, using the Matlab function “hinfsyn” [59].

$$\gamma = \begin{bmatrix} 0.9405 \\ 0.6727 \\ 0.8892 \end{bmatrix} \dots\dots\dots (4.42)$$

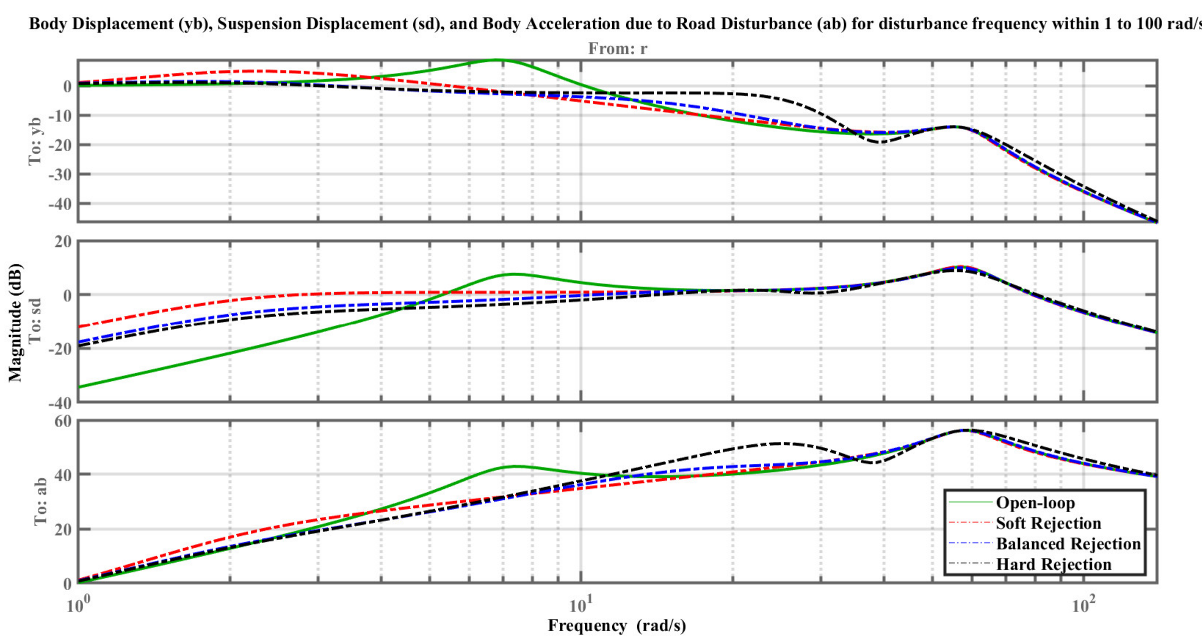

Fig. 4.15 Open-loop vs Closed-loop Response of the Active Suspension System

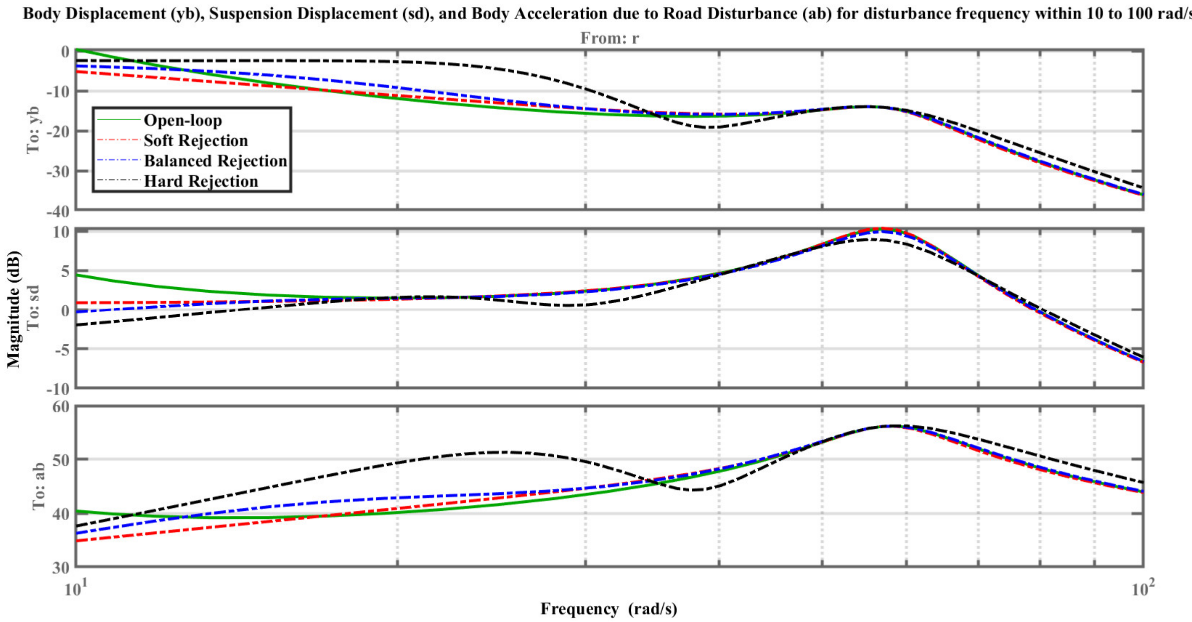

Fig. 4.16 Open-loop vs Closed-loop Response of the Active Suspension System (10 to 100 rad/s for disturbance)

Fig. 4.15 shows the open-loop response of the modeled suspension system being actuated by the EHSS subjected to road disturbances against the closed-loop performance for the three specified disturbance rejection criterion following the H∞ finite frequency robust control.

The performance indicator, γ in equation 4.42, presents the gain from road disturbance to Body displacement, y_b, suspension displacement s_d and body acceleration a_b to achieve the disturbance rejection which can be observed in Fig. 4.16 as well for the criterions of soft, balanced and hard rejections. The illustration also shows that the applied control technique reduces the body acceleration and suspension displacement below the model approximated deflection frequency of 23 rad/s as can be seen from Fig. 4.16. It is also evident that the body acceleration is smallest for the controller to achieve Soft rejection while the same is largest for the case of suspension displacement.

Thus, the balanced rejection is the best trade-off between these two parameters to achieve the best criteria for the active suspension system with the control objective of rejecting road disturbances occurring at higher deflection frequencies.

Chapter 5

Conclusion and Future Research Scope

5.1 Conclusion

The earlier investigations found that EHSS has non-minimum phase behavior based on its open-loop characteristics. Different control strategies had been adopted throughout the years to perfectly overcome the phase error caused by NMP features and also to curb the dead time in response. However, the majority of those studies were limited to EHSS modeling that was not subjected to parametric uncertainties caused by unknown internal model parameters and external load disruptions.

In this thesis, a mathematical model of an electro-hydraulic servo system (EHSS) is used to investigate the stability criteria utilizing software simulations. To determine the discrete time transfer function, the EHSS was originally provided with known model parameters. The system exhibited non-minimum phase phenomena owing to one of the two zeroes being outside of the unit circle of the z-plane, as determined by the open-loop pole and zero locations on the z-plane acquired from the EHSS's discrete time transfer function. The EHSS was also shown to be marginally stable, since two poles were found to be slightly beyond the unit circle of the z-plane. To improve the stability criterion for the EHSS suffering from NMP characteristics with known model parameters as had been studied so far, an optimal controller was designed by mathematically modeling a discrete linear quadratic regulator (DLQR). The closed-loop discrete time transfer function of the EHSS being controlled by the DLQR optimum controller was derived using the DLQR feedback gain. The pole zero locations of the DLQR controlled closed-loop EHSS were studied and it was found that all of the poles were pushed towards the unit circle of the z-plane. As a result, it was understood that the DLQR optimization was able to improve the stability of the EHSS response significantly, making the overall response to be stable. On the other hand, the location of one of the zeros of the closed-loop EHSS was still beyond the unit circle of the z-plane with the DLQR controller applied. Thus, it was determined that the DLQR optimum controller may improve the relative stability of the EHSS, but that the NMP features were caused by unknown model parameters.

In this way, the EHSS was comprehensively modeled, taking into consideration the impacts of internal leakages as well as external load disturbances. It was feasible to identify the parameters that contributed to the unpredictability of load displacement in relation to spool-valve displacement. The EHSS was studied to drive an active suspension load, and a disturbance rejection strategy technique was proposed to estimate the disturbance occurrence limitations The finite frequency robust control technique was then adopted to reject the external load disturbance through simulation for the already assumed approximated constraints. By setting various rejection performance criterions, simulation results demonstrated that the finite frequency robust control approach was able to reject disturbances. As a result, the optimal trade-off with the control goal of rejecting disturbances was accomplished, and the EHSS adversities of parametric uncertainties were overcome.

5.2 Future Works

The advancements in the EHSS stability criterion with known model parameters can be employed in subsequent research to get better control abilities. The use of EHSS for trajectory or position tracking is critical for efficient and optimal industrial applications, as it requires the system to be phase error-free. The proposed DLQR controlled EHSS can be studied further in accordance with other control strategies, such as a feed-forward controller to resolve the phase error problem, resulting in NMP behavior, which is vital in achieving perfect trajectory tracking control and facilitates easy operation in real-world scenarios.

A Finite $H\infty$ disturbance observer may be used to monitor the entire EHSS mathematical model and optimize the best feedback gain by rejecting the impacts of external disturbances. Experiments to assess the viability of this approach in real-world engineering scenarios for further refinement of parameter errors and disturbance input, as well as the targeted addition of additional control techniques for the enhanced actuation of Spool-valve displacement of EHSS invoking stable response in aerospace and automobile industrial applications, are one of the promising future research areas.

References

[1] X. Wang, Y. Feng and Y. Sun, "Research on improved active disturbance rejection control of continuous rotary motor electro-hydraulic servo system," *J. Cent. South Univ.,* no. 27, p. 3733–3743, 2020.

[2] Y. Bin , Z. Qixin , Y. Jing , Z. Junxiao , H. Zhipeng , J. Zhengguo and W. Xiangji , "Design, Mathematical Modeling and Force Control for Electro-Hydraulic Servo System With Pump-Valve Compound Drive," *IEEE Access,* vol. 8, pp. 171988-172005, 2020.

[3] L. Litong , C. Zheng and Y. Bin , "Advanced Valves and Pump Coordinated Hydraulic Control Design to Simultaneously Achieve High Accuracy and High Efficiency,," *IEEE Transactions on Control Systems Technology,* vol. 29, no. 1, pp. 236-248, 2021.

[4] Y. Zhikai , Y. Jianyong , Y. Feiyu , X. Qiang , X. Minrui and D. Wenxiang , "Model reference adaptive tracking control for hydraulic servo systems with nonlinear neural-networks," *ISA Transactions,* vol. 100, pp. 396-404, 2020.

[5] J. Xinhao , W. Chengwen , Z. Zhenyang , C. Shuai and G. Xinping , "Nonlinear adaptive position control of hydraulic servo system based on sliding mode back-stepping design method," *Journal of Systems and Control Engineering,* vol. 235, no. 4, pp. 474-485, 2020.

[6] A. Kabanov, "Feedback Linearization of Nonlinear Singularly Perturbed Systems with State-dependent Coefficients," *Int. J. Control Autom. Syst.,* vol. 18, p. 1743–1750, 2020.

[7] H. Lee and V. I. Utkin, "Chattering suppression methods in sliding mode control systems," *Annual Reviews in Control,* vol. 31, no. 2, pp. 179-188, 2007.

[8] R. Ghazali, Y. M. Sam, M. F. Rahmat and A. W. I. M. Hashim, "Simulation and Experimental Studies on Perfect Tracking Optimal Control of an Electrohydraulic Actuator System," *Journal of Control Science and Engineering,* vol. 2012, p. 8, 2012.

[9] L. Feng and H. Yan, "Nonlinear Adaptive Robust Control of the Electro-Hydraulic Servo System," *Appl. Sci.,* vol. 10, p. 4494, 2020.

[10] L. B. Prasad, B. Tyagi and H. O. Gupta, "Modelling and Simulation for Optimal Control of Nonlinear Inverted Pendulum Dynamical System Using PID Controller and LQR," in *Proceedings of the 2012 Sixth Asia Modelling Symposium*, Washington, DC, United States, 2012.

[11] L. Yin , J. Yao and Z. Yao, "Finite Frequency H∞ Control for Electro-Hydraulic Servo System With Parameter Uncertainties," in *5th International Conference on Advanced Robotics and Mechatronics (ICARM)*, Shenzhen, China, 2020.

[12] L. Wang and J. Cheng, "Robust disturbance rejection methodology for unstable non-minimum phase systems via disturbance observer," *ISA Transactions,* vol. 100, 2020.

[13] M. H. Nguyen, H. V. Dao and K. K. Ahn, "Active Disturbance Rejection Control for Position Tracking of Electro-Hydraulic Servo Systems under Modeling Uncertainty and External Load," *Actuators,* vol. 10, no. 2, p. 20, 2021.

[14] N. Novak, S. Vladimir and D. Vladimir, "Optimal control of hydraulically driven parallel robot platform based on firefly algorithm," *Nonlinear Dyn.,* vol. 82, p. 1457–1473, 2015.

[15] J. R. Jagat, D. Michael, R. K. Hamid and C. V. Kalyana, "Output feedback active suspension control with higher order terminal sliding mode," *IEEE Trans. Ind. Electron.,* vol. 64, p. 1392–1403, 2017.

[16] Y. Ye, C. B. Yin , Y. Gong and J. J. Zhou , "Position control of nonlinear hydraulic system using an improved PSO based PID controller," *Mech. Syst. Signal Pr.,* vol. 83, p. 241–259, 2017.

[17] B. Yao , F. P. Bu , R. John and T. C. George , "Adaptive robust motion control of single-rod hydraulic actuators: Theory and experiments," *IEEE-ASME Trans. Mech.,* vol. 5, no. 9, p. 79, 2000.

[18] R. C. Dorf and R. H. Bishop, Modern Control Systems, Delhi: Pearson India, 2008.

[19] B. Barra, M. El-Khoury and M. Fernández, "On undershoot in scalar discrete-time systems," *Automatica,* vol. 32, no. 2, pp. 255-259, 1996.

[20] H. Khalil, Nonlinear Systems, New Jersey: Prentice Hall, Upper Saddle River, USA, 2002.

[21] M. Kalyoncu and H. Mustafa , "Mathematical modelling and fuzzy logic based position control of an electrohydraulic servo system with internal leakage," *Mechatronics,* vol. 19, no. 6, pp. 847-858, 2009.

[22] R. Ghazali, Y. M. Sam, M. F. Rahmat, A. W. Zulfatman and I. M. Hashim, "Perfect Tracking Control with Discrete-time LQR for a Non-minimum phase Electro-Hydraulic Actuator System," *International Journal on Smart Sensing and Intelligent Systems,* vol. 4, no. 3, 2011.

[23] M. Basseville and I. Nikiforov, Detection of Abrupt Changes, Englewood Cliffs: Prentice Hall, 1993.

[24] M. I. Ahmed and A. Azad, "Mathematical modeling and DLQR based controller design for a non-minimum phase Electro Hydraulic Servo system (EHS)," in *2016 IEEE Region 10 Conference (TENCON)*, Singapore, 2017.

[25] R. Ghazali, C. C. Soon , H. I. Jaafar, Y. M. Sam and M. F. Rahmat, "System Identification of Electro-hydraulic Actuator System with Pressure and Load Effects," in *IEEE International Conference on Control System, Computing and Engineering*, Penang, Malaysia, 2014.

[26] R. Adnan, A. M. Samad and M. M. Mustafa, "Real-Time Control of Non-Minimum Phase Electro-Hydraulic System Using Trajectory Adaptive ZPETC," in *IEEE 7th International Colloquium on Signal Processing and its Applications*, Penang, Malaysia, 2011.

[27] G. Franklin, J. D. Powell and A. Emami-Naeini, Feedback Control of Dynamic Systems, Singapore: Pearson Education (Singapore) Pte. Ltd., 2002.

[28] A. Jezierski, J. Mozaryn and D. Suski, "A Comparison of LQR and MPC Control Algorithms of an Inverted Pendulum," in *Mitkowski W., Kacprzyk J., Oprzędkiewicz K., Skruch P. (eds) Trends in Advanced Intelligent Control, Optimization and Automation*, Springer, Cham, 2017, pp. 65-76.

[29] E. Shojaei Barjuei and J. Ortiz, "A comprehensive performance comparison of linear quadratic regulator (LQR) controller, model predictive controller (MPC), H∞ loop

shaping and μ-synthesis on spatial compliant link-manipulators," *Int. J. Dynam. Control,* vol. 9, pp. 121-140, 2021.

[30] E. F. Ferreira, V. F. João and J. V. F. Neto, "Numerical stability improvements of state-value function approximations based on RLS learning for online HDP-DLQR control system design," *Engineering Applications of Artificial Intelligence,* vol. 63, pp. 1-19, 2017.

[31] L. Fan, P. Liu, H. Teng, G. Qiu and P. Jiang, "Design of LQR Tracking Controller Combined With Orthogonal Collocation State Planning for Process Optimal Control," *IEEE Access,* vol. 8, pp. 223905-223917, 2020.

[32] J. Yong and X. Y. Zhou, Stochastic Control: Hamiltonian Systems and HJB Equations, New York, USA: Springer - Science+Business Media, LLC, 1999.

[33] H. J. Sussmann and J. C. Willems, "300 Years of Optimal Control: From Brachystochrone to the Maximum Principle," *IEEE Control Systems,* vol. 17, no. 3, pp. 32-44, 1999.

[34] S. Morita, "Intuitive Concept or Physical Meaning of Lagrangian," *World Journal of Mechanics,* vol. 6, pp. 84-93, 2016.

[35] R. Ghazali, Y. M. Sam, M. F. Rahmat, Zulfatman and A. W. I. M. Hashim, "Point-to-Point Trajectory Tracking with Two-Degree-ofFreedom Robust Control for a Non-minimum Phase Electro-hydraulic System," in *10th World Congress on Intelligent Control and Automation*, Beijing, 2011.

[36] I. The MathWorks, "c2d: Convert model from continuous to discrete time," The MathWorks, Inc., June 2021. [Online]. Available: https://www.mathworks.com/help/control/ref/lti.c2d.html. [Accessed 25 June 2021].

[37] M. Kalyoncu and M. Haydim, "Mathematical modelling and fuzzy logic based position control of an electrohydraulic servosystem with internal leakage," *Mechatronics,* vol. 19, no. 6, pp. 847-858, 2009.

[38] B. Eryılmaz and B. H. Wilson, "Modeling the Internal Leakage of Hydraulic Servovalves," in *Proceedings of the ASME dynamic systems and control division, ASME international mechanical engineering congress and exposition*, 2000.

[39] W. J. Thayer, "Specification Standards for Electrohydraulic Flow Control Servovalves," Moog Inc. Technical Report 117, 1962.

[40] J. S. Yun and H. S. Cho, "Application of an Adaptive Model Following Control Technique to a Hydraulic Servo System subjected to Unknown Disturbances," *Journal of Dynamic Systems, Measurement and Control,* vol. 113, no. 3, pp. 479-486, 1991.

[41] M. G. Rabie, Fluid Power Engineering, New York, USA: McGraw Hill, 2009.

[42] A. (. v. Schijndel, "A review of the application of SimuLink S-functions to multi domain modelling and building simulation," *Journal of Building Performance Simulation,* vol. 7, no. 3, pp. 165-178, 2014.

[43] S. Mikkili, A. K. Panda and J. Prattipati, "Review of Real-Time Simulator and the Steps Involved for Implementation of a Model from MATLAB/SIMULINK to Real-Time," *J. Inst. Eng. India Ser. B ,* vol. 96, p. 179–196, 2015.

[44] J. Hu and Y. Qiu, "Performance-oriented asymptotic tracking control of hydraulic systems with radial basis function network disturbance observer," *Advances in Mechanical Engineering,* vol. 8, no. 6, p. 1–12, 2016.

[45] S. DRAKUNOV, G. D. HANCHIN, W. C. SU and Ü. ÖZGÜNER, "Nonlinear Control of a Rodless Pneumatic Servoactuator, or Sliding Modes versus Coulomb Friction," *Automatica,* vol. 33, no. 7, pp. 1401-1408, 1997.

[46] W. Deng, J. Yao and Z. Jiao, "Adaptive backstepping motion control of hydraulic actuators with velocity and acceleration constraints," in *Proceedings of the 2014 IEEE Chinese guidance, navigation and control conference (CGNCC)*, Yantai, China, 2014.

[47] K. Guo, J. Wei and Q. Tian, "Disturbance observer based position tracking of electro-hydraulic actuator," *J. Cent. South Univ.,* vol. 22, p. 2158–2165 , 2015.

[48] J. Yao, Z. Jiao and D. Ma, "A Practical Nonlinear Adaptive Control of Hydraulic Servomechanisms With Periodic-Like Disturbances," *IEEE/ASME Transactions on Mechatronics,* vol. 20, no. 6, pp. 2752-2760, 2015.

[49] J. Yao, W. Deng and Z. Jiao, "Adaptive control of hydraulic actuators with LuGre model-based friction compensation," *IEEE T Ind Electron,* vol. 62, p. 6469–6477, 2015.

[50] Y. Hong and B. Yao, "A Globally Stable High-Performance Adaptive Robust Control Algorithm With Input Saturation for Precision Motion Control of Linear Motor Drive Systems," *IEEE/ASME Transactions on Mechatronics,* vol. 12, no. 2, pp. 198-207, 2007.

[51] G. Yang, J. Yao and G. Le, "Adaptive robust control of DC motors with time-varying output constraints," in *Proceedings of the 2015 34th Chinese control conference*, Hangzhou, China, 2015.

[52] H. Jing, R. Wang, C. Li and J. Bao, "Robust finite-frequency H∞ control of full-car active suspension," *Journal of Sound and Vibration,* vol. 441, pp. 221-239, 2019.

[53] Z. Zhang , H. Li, C. Wu and Q. Zhou, "Finite frequency fuzzy H∞ control for uncertain active suspension systems with sensor failure," *IEEE/CAA Journal of Automatica Sinica,* vol. 5, no. 4, pp. 777-786, 2018.

[54] W. Sun, Y. Zhao, J. Li, L. Zhang and H. Gao, "Active suspension control with frequency band constraints and actuator input delay," *IEEE Transactions on Industrial Electronics,* vol. 59, no. 1, pp. 530-537, 2012.

[55] M. Inc., "Robust Control Toolbox," Mathworks Inc., 2021. [Online]. Available: https://www.mathworks.com/help/robust/index.html?s_tid=CRUX_lftnav. [Accessed 26 July 2021].

[56] D. Wang, D. Zhao, M. Gong and B. Yang, "Research on Robust Model Predictive Control for Electro-Hydraulic Servo Active Suspension Systems," *IEEE Accrss,* vol. 6, pp. 3231-3240, 2018.

[57] M. Inc., "Robust Control of an Active Suspension," Mathworks Inc., 2021. [Online]. Available: https://www.mathworks.com/help/robust/gs/active-suspension-control-design.html. [Accessed 26 July 2021].

[58] M. Inc., "ultidyn," Mathworks Inc., 2021. [Online]. Available: https://www.mathworks.com/help/robust/ref/ultidyn.html. [Accessed 17 August 2021].

[59] M. Inc., "hinfsyn," Mathworks Inc., 2021. [Online]. Available: https://www.mathworks.com/help/robust/ref/lti.hinfsyn.html?s_tid=doc_ta#mw_4d02a4ff-a6f3-4c1e-90ae-9d5f0d57ec31. [Accessed 17 August 2021].

Appendix A

Dataset for the Comprehensive EHSS SIMULINK Work

```
% Current gain Ki
Ki=0.556
% Armature damping coefficient fth
fth=0.002
% Moment of inertia of rotor J(kg sqm)
J=5e-7
% Armature rotational angle torque gain Kth
Kth=9.45e-4
% Flexible tube rotational stiffness KT
KT=10
% Flapper length Lf(m)
Lf=0.009
% Mechanical feedback spring length Ls(m)
Ls=0.03
% Flapper limiting displacement xi(m)
xi=30e-6
% pi
pi=3.14159
% flapper diameter df(m)
df=0.0005
% Flapper nozzle area Af (sq m)
Af=pi*df*df/4
% Equivalent flapper seat material damping coefficient Rf(Nsm)
Rf=5000
% Flapper seat equivalent stiffness KLf(N/m)
KLf=5e6
% Oil density Ro (kg/Cum)
Ro=867
% Cd*(2/Ro)^0.5
Cdro=0.611*(2/Ro)^0.5
% Hydraulic amplifier nozzles N1 & N2 diameter dfn(m)
dfn=0.0005
% Diameter of return orifice N5 d5(m)
d5=0.0006
% Flapper valve nozzele 1 & 2 area AN(sq m)
AN=pi*dfn*dfn/4
% Flow Coefficients (in SI)
C12=Cdro*AN
C34=Cdro*pi*df
C5=Cdro*pi*d5*d5/4
% Spool diameter ds (m)
%ds=0.0046
ds=.004621398070216039
% Spool area As (sq m)
As=pi*ds*ds/4
```

```
% Initial volume of oil in spool side chamber Vo (Cu m)
Vo=2e-6
% Bulk modulus os oil B (Pa)
B=1.5e9
% Initial Volume of oil in the retutn chambet (Cu m)
V3=5e-6
% Spool mass ms (kg)
ms=0.02
% Spool Damping coefficient fs (Ns/m)
fs=2
% Feedback spring stiffness (N/m)
Ks=900
% Supply Pressure Ps (Pa)
Ps=2e7
% Return Pressure Pt (Pa)
Pt=0
% Servoactuator feedback gain kfb (A/m)
kfb=3
% Spool port width Omiga Omiga (m)
Omiga=0.002
% Spool radial clearance c (m)
c=2e-6
% Piston area Ap (Sq m)
Ap=1.25e-3
% Initial volume of oil in cylinder chamber Vc (Cu m)
Vc=100e-6
% Resistance to internal leakage
Ri=1e20
% Piston mass mp (kg)
mp=10
% Friction coefficient on piston
fp=1000
% Piston loading coefficient Ky
Ky=0
```

Appendix B

B.1: m-file MATLAB code for computing the DLQR gain

```
%% Model parameters for EHSS

Ps = 7e6;  %Pressure applied across  load
Ap = 3e-4; %Surface area of piston
Ctp = 2e-12; %Total leakage co-efficient of Piston
betae = 700; %Effective Bulk modulus (Compressibility)
Vt = 6e-5; %Total Compressed Oil Volume
Mt = 250; %Mass of Piston
Bt = 100; %Damping co-efficient of Piston
Kq = 2.2e-6; %Flow gain co-efficient

%% Simplifying the Computation of model parameters
NN = Ctp;
XX = (Vt*Mt);
WW = (4*betae);
QQ = sqrt(WW./XX);
ZZ = (Mt.*NN);
YY = (2*Ap^2);

Wn = Ap.*QQ;
zeta = ZZ./YY;
K = Kq./Ap;

%% Continuous time transfer of the EHS system

Gc = tf([0 0 0 K.*Wn^2],[1 2.*zeta.*Wn Wn^2 0]);
Gd = c2d(Gc,10,'zoh') % Corresponding discrete time transfer function
sys = idss(Gd); % State space identified model
pzmap(sys) % pole zero plot of the Open-loop system % NMP

[A,B,C,D] = ssdata(sys); % State space matrices obtained from the discrete
time transfer function
figure(2); step(Gd,100) % Step response of the EHS system

%% DLQR controller design

rho = 0.1;
Q = C*C'.*rho;
R = 1;
k = DLQRO(A,B,C,Q,R) % Using DLQRO command, detailed in Appendix B, B.2

%% Closed-loop trnasfer function xdot(n) = (A-BK)x(n)

Hx = ss(A-(B*k),B(:,1)*k(1,:),C,0);
[E,F,G,H] = ssdata(Hx)
[b,a] = ss2tf(E,F,G,H,1);
SYS_cl = tf(b,a);
Hd = c2d(Hx,10,'zoh')
sysHd = idss(Hd)
figure(3); step(Hx,100) % Step response of the system associating the DLQR
regulator
figure (4); pzmap(sysHd) % pole zero plot after DLQR application
```

B.2: m-file MATLAB function code for DLQRO

```
function k = dlqro(a,b,c,q,r)
%DLQRO Linear Quadratic Regulator Design for Diacrete Time Systems
%       K = DLQRO(A,B,C,Q,R) calculates the optimal feedback gain matrix K
%       Such that the feedback law
%           u = - Kx
%
%       Minimizes the cost function:
%
%           J = Sum {y'Q'Qy + u'R'Ru}
%
%       Subject to the constraint equation:
%
%           x[n+1] = Ax[n] + Bu[n]

error(nargchk(5,5,nargin));
error(abcdchk(a,b,c));

[mc,nc] = size(c);
[mb,nb] = size(b);
[mq,nq] = size(q);
if (mc ~= mq)
    error('C and Q must be consistent')
end

[n,m] = size(b);
nn = m+n;
p = c+q;
u = [r zeros(m,n)];
for i = 1:40
    d = [u(1:m,:);p*b p*a];
    [t,u] = qr(d);
    p = u(m+1:2*m,m+1:nn);
end
k = u(1:m,1:m)\u(1:m,m+1:nn);
```

Appendix C

Detailed SIMULINK Block Diagrams

C.1 SIMULINK Block Diagram of Armature Dynamics of the Torque Motor

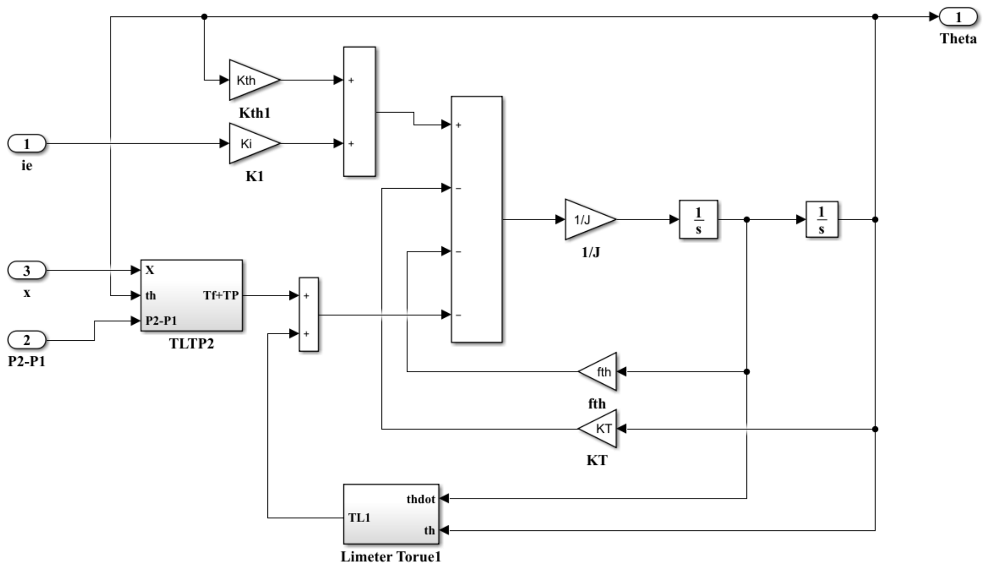

C.2 SIMULINK Block Diagram of Spool Pressure Dynamics

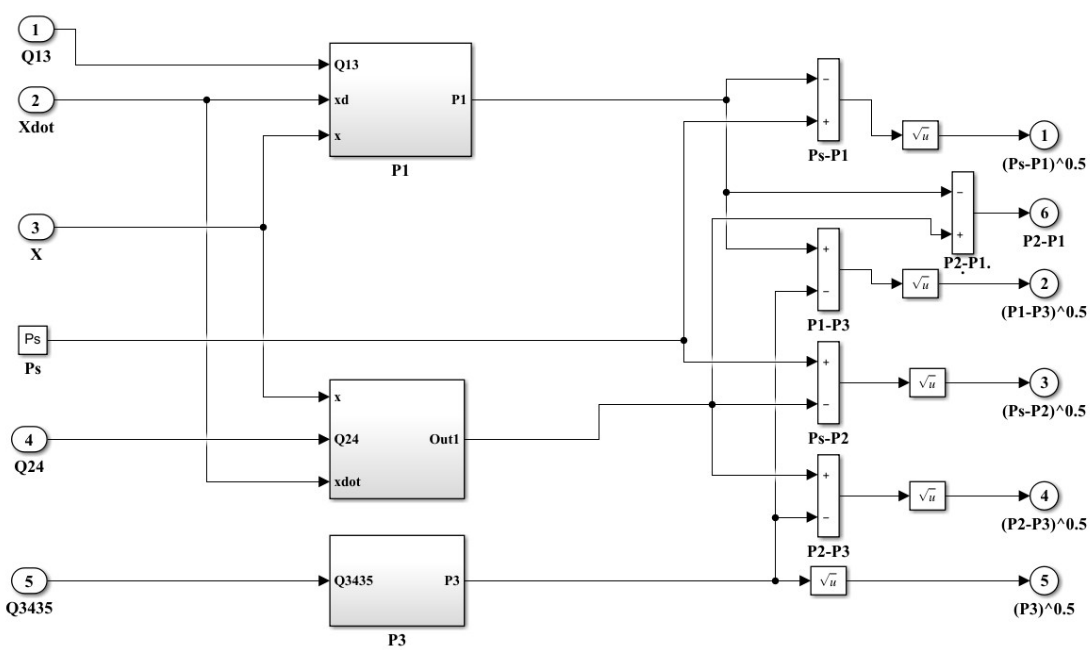

C.3 SIMULINK Block Diagram of Flow rate Dynamics

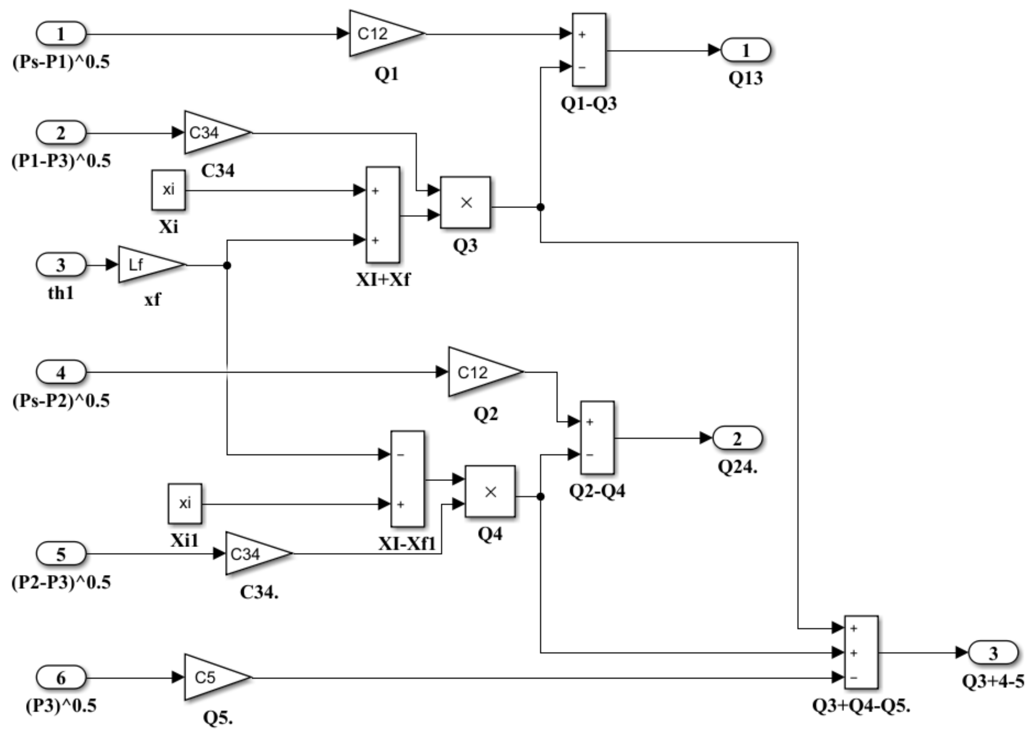

C.4 SIMULINK Block Diagram of Spool-valve Displacement Dynamics